

Earthquake swarm and *b*-value characterization of the Yellowstone volcano-tectonic system

Jamie Farrell ^{a,*}, Stephan Husen ^b, Robert B. Smith ^a

^a University of Utah Dept. of Geology and Geophysics, Salt Lake City, UT, 84112, USA

^b Swiss Seismological Service, ETH Zurich, CH8092 Zurich, Switzerland

ARTICLE INFO

Article history:

Received 30 October 2008

Accepted 15 August 2009

Available online 25 August 2009

Keywords:

Yellowstone

b-value

earthquake swarm

seismicity

volcano

ABSTRACT

The Yellowstone volcanic field, Yellowstone National Park, is one of the most seismically active areas of the western U.S., experiencing the deadly 1959 $M7.5$ Hebgen Lake, MT, earthquake adjacent to the 0.64-Ma caldera, as well as more than 30,000 earthquakes from 1973 to 2007. This well-recorded seismic activity offers the opportunity to study the temporal and spatial occurrence of earthquakes and extensive earthquake swarms and how they relate to active volcanic and tectonic processes. We characterize the distribution of earthquakes by analyzing the rate of occurrence characterized by the *b*-value. To accurately determine *b*-values, the earthquake catalog was filtered to identify statistically time- and spatially-dependent related events, defined as swarms, from independent single main and aftershocks. An algorithm was employed that identified 69 swarms for 1984–2006 based on inter-event times and spatial clustering. The swarms varied in duration from 1 to 46 days with the number of events varying from 30 to 722 with magnitudes of -1.2 to 4.8 . All of the swarm events as well as the 597 events triggered by the 2002 Denali fault, AK, earthquake were removed from the catalog for analysis. The catalog data were then filtered for a magnitude of completeness (M_{COMP}) of 1.5 and the *b*-value distribution for the Yellowstone region was determined with the de-swarmed data. *b*-values ranged from 0.6 ± 0.1 to 1.5 ± 0.05 with the highest values associated with the youthful 150,000-year old Mallard Lake resurgent dome. These variations are interpreted to be related to variations in stresses accompanying the migration of magmatic and hydrothermal fluids. An area of high *b*-values (up to 1.3 ± 0.1) associated with the Hebgen Lake fault zone west of the Yellowstone caldera could be related to the transport of magmatic fluids out of the Yellowstone volcanic system or could be indicative of a relative low stress regime resulting from the stress release by the Hebgen Lake earthquake. An area of low *b*-values (0.6 ± 0.1) south of the Yellowstone caldera is interpreted as evidence of a relatively higher stress regime associated with an area of dominantly extensional stress. This seismicity was associated with a nearly 90° change in the principal stress axes direction to northeast-southwest, compared to east-west within the Yellowstone caldera, and may be influenced by buoyancy loading by the Yellowstone hotspot.

© 2009 Elsevier B.V. All rights reserved.

1. Introduction

The Yellowstone Plateau, centered on Yellowstone National Park, WY, ID, and MT, reflects an area of widespread hydrothermal features and Quaternary silicic volcanism characterized by three giant caldera-forming eruptions (Christiansen, 1984, 2001), extensive post-caldera rhyolitic eruptions as young as 70,000 years ago (Christiansen, 1984, 2001), in addition extraordinarily high heat flow ($>2000\text{ mW/m}^2$) (Morgan et al., 1977; DeNosaquo et al., 2009-this volume), unprecedented high rates of modern crustal deformation, and a well seismically defined crustal magma chamber and extensive seismicity (Smith et al., 2009-this volume) characterize the system. Thirty-three years of seismic recording by the Yellowstone seismic network has

allowed the assessment of the frequency of earthquake occurrence, characterized by *b*-values, that were then correlated with active volcanic and tectonic features.

The *b*-value is a measure of the relative number of small to large earthquakes that occur in a given area in a given time period. In particular, the *b*-value is the slope of the frequency-magnitude distribution (Ishimoto and Iida, 1939; Gutenberg and Richter, 1944) for a given population of earthquakes. Studies have shown that the *b*-value changes with material heterogeneity (Mogi, 1962), thermal gradient (Warren and Latham, 1970), and applied stress (Scholz, 1968; Wyss, 1973; Urbancic et al., 1992; Schorlemmer et al., 2004; Schorlemmer and Wiemer, 2005; Schorlemmer et al., 2005). In tectonic areas, the *b*-value is generally around 1.0 (Frolich and Davis, 1993). In contrast, volcanic areas are characterized by *b*-values greater or less than 1.0 with values as high as 3.0 (McNutt, 2005).

Over 30,000 earthquakes, $-0.5 < M_C \leq 6$, have been recorded in the Yellowstone area since 1973 (Fig. 1). This earthquake data set offers the opportunity to study the temporal and spatial occurrence of

* Corresponding author.

E-mail address: farrell@earth.utah.edu (J. Farrell).

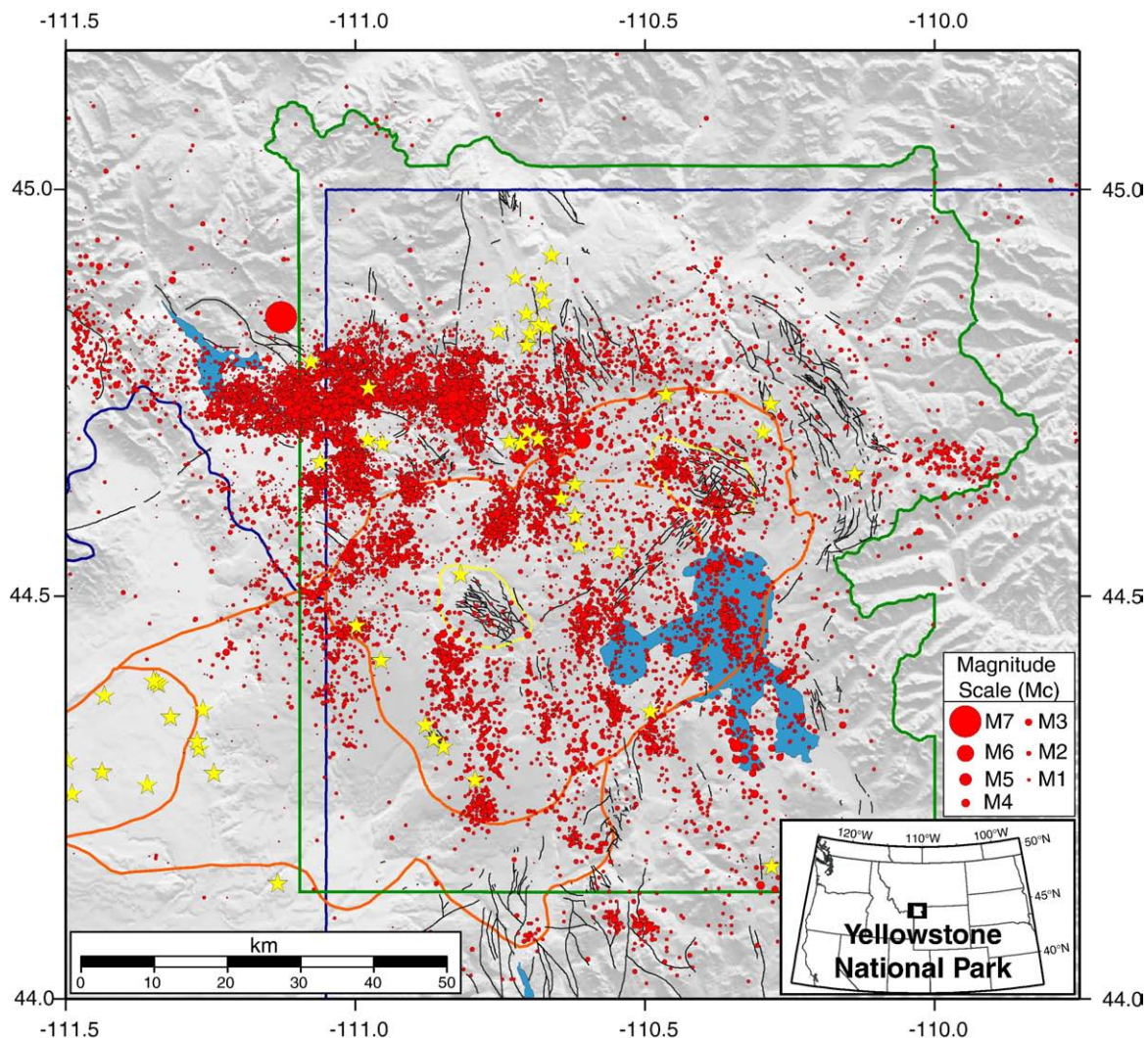


Fig. 1. Earthquakes of the Yellowstone region from 1973 to 1981 and 1984 to 2006 (1973–2004: Husen and Smith, 2004; 2005–2006: this study), draped on gray-shaded relief topographic map. Epicenters are shown as red dots, post 0.64-Ma caldera vents are shown as yellow stars, and Late Quaternary faults are shown as black lines. The outlines of the calderas from the last three major Yellowstone eruptions are shown in orange. The Mallard Lake (south) and Sour Creek (north) resurgent domes are outlined in yellow. State boundaries are shown as blue lines and Yellowstone National Park is outlined in green. Volcanic vents, caldera outlines, and Quaternary faults are from Christiansen (2001).

earthquakes, parameterized by the b -value, which is the slope of the earthquake recurrence curve. The Gutenberg–Richter relationship is the commonly assumed frequency of occurrence distribution that assumes a Poisson (random) distribution of earthquake magnitudes assuming that all dependent (non-random) events must first be removed from the catalog. Dependent events include foreshocks, aftershocks, earthquake swarms, and triggered events. It has been suggested that earthquake swarms occur because of stress perturbations associated with the migration of magmatic or hydrothermal fluids through new or previously formed crustal inhomogeneities including crustal fractures (Hill, 1977; Toda et al., 2002; Waite and Smith, 2002) or because of aseismic slip and fluid pressure variations (Vidale et al., 2006).

Seismicity in Yellowstone is dominated by earthquake swarms, generally defined as the spatial and temporal clustering of earthquakes without an outstanding event of magnitude greater than one unit from the swarm average. Thus it is imperative to accurately identify earthquake swarms before calculating b -values. The combination of the high seismicity and distinct swarm activity, the complex volcanic and tectonic setting, and dynamic nature of the Yellowstone system suggest that spatial as well as temporal changes in the b -value may be an important characteristic of the volcano-tectonic system. This analysis, however, requires accurate hypocenter locations.

The data used here are a subset of the high-precision data determined by Husen and Smith (2004) of relocated hypocenters determined using tomographically determined three-dimensional P-wave velocity models for seismicity from 1973 to 2002. Hypocenters for the later period, 2003–2006, were relocated using the velocity model for the time period 1995–2002 of Husen and Smith (2004) and added to the catalog providing a total of 29,336 earthquakes.

The events were then classified into four quality classes: A, B, C, and D based on the Root Mean Square (RMS), the difference (in km) between the expected (the linearized location) and the maximum likelihood hypocenter location, and the average location error as approximated by the 68% confidence ellipsoid (Husen and Smith, 2004). Standardized magnitudes were recalculated by the coda lengths, defined as the Coda magnitudes (M_C) using available instrument calibrations and an improved magnitude equation from Pechmann et al. (2001):

$$M_C = -2.60 + 2.44 \log \tau + 0.0040\Delta \quad (1)$$

where τ is signal duration in seconds measured on a short-period vertical component seismogram, and Δ is epicentral distance in kilometers.

Because of the elimination of previous systematic time-dependent magnitude shifts, the recomputed M_C values are considered more consistent and reliable than previous M_C estimations. Essentially all the earthquakes in the catalog have magnitudes less than or equal to $M_C = 4.0$; 99.1% have $M_C \leq 3.0$; 91.2% have $M_C \leq 2.0$; and 53.6% have $M_C \leq 1.0$. Because of the importance of high quality locations and well-constrained magnitudes in calculating b -values, only A, B, or C quality events were used because they have RMS values less than 0.5 s. A total of 123 quality D events were rejected from the analysis ranging in magnitude from less than 0 to 3.5. Also, only earthquakes from 1984 to 2006 were used in this study because of the more consistent and reliable nature of the magnitudes due to improved digital monitoring and geographic network coverage with more instruments. This left 23,054 events in the data set hereafter referred to as the catalog of earthquakes. The average M_C for the time period of 1984 to 2006 is 1.0, and only 10% of the earthquakes have $M_C > 2.0$.

Earthquake swarms were then identified and were removed from the dataset using the algorithm from Waite (1999) in which swarms are identified based on an inter-event time and a distance between two related events. Earthquakes triggered by the M7.9 2002 Denali fault earthquake (Husen et al., 2004b; Husen et al., 2004c) were also identified and removed from the data. The magnitude of completeness was then calculated for different spatial and temporal subsets and the catalog was cut at the highest magnitude of completeness value. The remaining events were used to calculate the b -value distribution for the Yellowstone volcanic–tectonic system.

A total of 69 distinct earthquake swarms were identified comprising 8924 earthquakes, or 39% of the total number of earthquakes from 1984–2006. These events were also removed from the catalog that was limited to the threshold of completeness of $M_C = 1.5$. The remaining 2747 earthquakes were used to calculate b -values. Results show that the b -value varies laterally in Yellowstone from 1.5 ± 0.05 near the Mallard Lake resurgent dome to 0.6 ± 0.1 south of the Yellowstone caldera near the Mt. Sheridan fault and the northern segment of the Teton fault.

2. Geological setting and seismicity in Yellowstone

The Yellowstone volcanic system is one of the largest active silicic volcanic systems in the world (Christiansen, 2001). It forms a topographically high plateau of ~500 m excess elevation relative to the Basin-Range/Rocky Mountains as the result of mantle hotspot buoyancy (see summary by Smith et al., 2009-this volume). The youthful volcanic history of Yellowstone is dominated by three cataclysmic caldera-forming eruptions in the past two million years at 2.05, 1.3 and 0.64 Ma (Christiansen, 2001). The latest eruption (0.64 Ma) created what is subsequently referred to as the Yellowstone caldera, which extends 40×60 km (Fig. 2). Two structural resurgent domes formed after the caldera eruptions: the Mallard Lake resurgent dome in the southwestern portion of the Yellowstone caldera and the Sour Creek resurgent dome in the northeast part of the Yellowstone caldera (Fig. 2). In the last 640,000 years, at least 30 much smaller rhyolitic and basaltic flows as young as 70,000 years old have covered much of the Yellowstone Plateau.

With over 10,000 geysers, hot springs, and fumaroles, Yellowstone has the world's highest concentration of hydrothermal features reflecting its extraordinarily high convective ground water circulation (Fournier, 1989). The large hydrothermal systems are considered to be the result of hot water circulating along fractures in the crust heated by crystallizing magma (Fournier, 1989).

Four local earthquake tomography studies of Yellowstone (Benz and Smith, 1984; Lynch, 1999; Miller and Smith, 1999; Husen et al., 2004a) have imaged at various resolutions, with progressions in data access and expansion of the seismic network, a well defined low (~6%) V_p body in the upper crust beneath the Yellowstone caldera that has been interpreted as a body of 8–15% partial melt (Miller and

Smith, 1999; Husen et al., 2004a). By the addition of several three-component seismographs in the Yellowstone region, Husen et al. (2004a) was able to extend the earlier work by selecting 3374 local earthquakes between 1995 and 2001 and using 34,538 P-wave arrival times and 5875 S-P times to image the 3-D V_p and V_p/V_s structure of the upper crust beneath Yellowstone. Husen et al. (2004a) imaged a low (~10%) V_p body at ~2 km depth on the northwest boundary of the Yellowstone caldera as well as a low (~5%) V_p/V_s body in the same area. This low V_p and V_p/V_s body has been interpreted as a CO₂ gas-filled body (Husen et al., 2004a).

Crustal deformation monitoring of Yellowstone by precise spirit leveling and more recent Global Positioning System (GPS) and Interferometric Synthetic Aperture Radar (InSAR) measurements have shown unprecedented caldera uplift and subsidence during the last 80 years. This caldera-wide deformation includes uplift of up to 1 m from 1923 to 1984 measured by leveling (Pelton and Smith, 1982; Dzurisin et al., 1990). Beginning in 1987 the University of Utah began campaign GPS studies in the Yellowstone region and in 1996 data from continuous GPS stations were used to measure ground deformation. From 1987 to the present, ground deformation was measured from campaign and continuous GPS measurements. The results show that from 1987 to 1995 the Yellowstone caldera subsided at a maximum rate of -14 ± 3 mm/yr centered near the Sour Creek dome for a total of 112 mm. From 1995 to 2000 the Yellowstone caldera returned to uplift with a maximum rate of 15 ± 4 mm/yr for a total of 75 mm (Puskas et al., 2007). However the center of uplift during this time period was centered northwest of the Yellowstone caldera in the Norris–Mammoth corridor (Fig. 2). From 2000 to 2003 the uplift continued northwest of the Yellowstone caldera at a maximum rate of 12 ± 4 mm/yr for an additional 36 mm of displacement but the central caldera axis returned to subsidence at a maximum rate of -9 ± 6 mm/yr for an additional 27 mm subsidence (Puskas et al., 2007).

Remarkably, since late 2004, Yellowstone has been experiencing accelerated uplift of the 0.64-Ma caldera with rates up to 70 mm/yr, three times greater than previously observed deformation episodes (Chang et al., 2007). Source modeling of the deformation suggests a near-horizontal expanding magma body over an area 40×60 km², at 9 km beneath the Yellowstone caldera, notably located near the top of the seismically imaged crustal magma chamber. In addition, tens to hundreds of small earthquakes ($M < 3$) occurred during the deformation period and were concentrated within the modeled dilatation zone while the rest of the Yellowstone caldera experienced low seismicity (Chang et al., 2007).

Perhaps one of the most striking features of the Yellowstone Plateau is its extraordinarily high heatflow. The presence of crystallizing magma at shallow depths (~8 km) fuels the regional heat flow at Yellowstone by combined conduction and convection, estimated at more than 2000 mW/m² (Blackwell, 1969; Fournier, 1989; DeNosaquo et al., 2009-this volume), this is more than 30 times the continental average (Fournier, 1989). Given a conductive heat flow of ~200 mW/m², the Nusselt number (which is the ratio of convective heat flow and conductive heat flow) for the Yellowstone caldera is ~10. This compares to values of ~6 to 8 for the Long Valley caldera in eastern California (Hill, 1992).

The Yellowstone Plateau is one of the most seismically active areas of the western U.S. and is part of the distinct N–S band of intraplate seismicity known as the Intermountain seismic belt (Smith and Sbar, 1974; Smith and Arabasz, 1991) (Fig. 1). Moreover, the Yellowstone area has experienced the largest historic earthquake of the ISB: the August, $M_S 7.5$ 1959 Hebgen Lake, Montana event located ~25 km northwest of the Yellowstone caldera (Doser, 1985). The Yellowstone caldera has also experienced a $M_L 6.1$ earthquake in 1975 southeast of Norris Junction (Pitt et al., 1979; Smith and Arabasz, 1991).

Overall, seismic activity in Yellowstone is characterized by swarms of small, shallow earthquakes. Focal depths within the Yellowstone caldera are limited by high temperatures to the shallow depth of the brittle–ductile transition at 4–6 km and deepen to up to 18 km in the

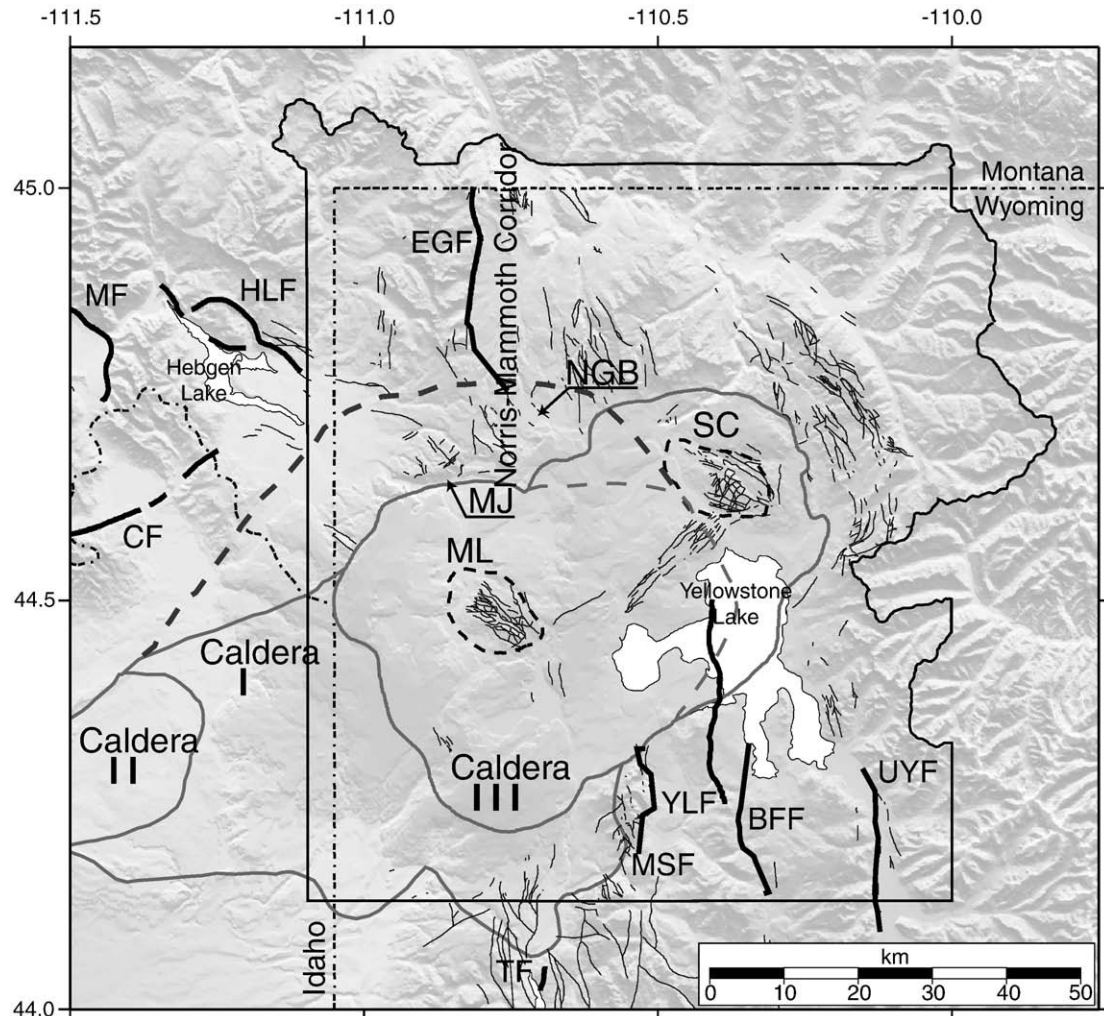


Fig. 2. Gray-shaded topographic relief map of the Yellowstone volcanic field showing calderas and Cenozoic faults after Christiansen (2001). Major faults are shown as thick black lines. MF = Madison fault, HLF = Hebgen Lake fault, CF = Centennial fault, EGF = East Gallatin fault, TF = Teton fault, MSF = Mt. Sheridan fault, YLF = Yellowstone Lake fault, BFF = Buffalo Fork fault, and UYF = Upper Yellowstone Valley fault. The Norris Geyser Basin location is shown as NGB. Madison Junction is shown as MJ. Calderas are shown by age: I – 2.05 Ma, II – 1.3 Ma, and III – 0.64 Ma. The bold gray dashed line outlines a region of highly fractured crust and high seismicity that may mark the extent of caldera I. The northern boundary of caldera I is highlighted by a topographic contrast that may have resulted from the 2.05 Ma catastrophic eruption. ML and SC represent the Mallard Lake and Sour Creek resurgent domes respectively, which are outlined with a dashed line (modified from Waite (1999)).

much cooler tectonic regime in the Hebgen Lake, MT area west of the Yellowstone caldera (Smith et al., 2009-this volume). The most intense seismicity extends from the Hebgen Lake area east to the northern Yellowstone caldera boundary near Norris Junction (Fig. 1). Although this area only constitutes 16% of the Yellowstone area, it contains 75% of the earthquakes from 1973 to 2006. Linear bands of epicenters within and adjacent to the Yellowstone caldera are aligned generally north-northwest parallel to alignments of post-caldera volcanic vents and large regional faults (Fig. 1). These normal faults are assumed to be buried at depth beneath young post-caldera rhyolite flows and are inferred to have once been continuous normal faults bounding mountain blocks of Basin-Range origin (Christiansen, 1984; Smith and Braile, 1994) (Fig. 2).

The largest earthquake swarm recorded in Yellowstone occurred in October of 1985 and consisted of over 3000 earthquakes ($M_c < 5$) that spanned more than 3 months (Waite and Smith, 2002). The temporal pattern of epicenters in the 1985 swarm was characterized by northwest migration away from the 0.64-Ma caldera at an average rate of 150 m/day. The swarm also coincided with a pronounced change of Yellowstone caldera uplift to subsidence. Waite and Smith (2002) suggested that the subsidence was partially accommodated by the migration of magma-derived fluids out of the Yellowstone caldera

toward the northwest. The most likely scenario explaining this process involves the rupture of a self-sealed hydrothermal layer and subsequent migration of hydrothermal fluids through a preexisting fracture zone out of the Yellowstone caldera, causing the earthquakes of the 1985 swarm (Waite and Smith, 2002).

The second largest swarm recorded in Yellowstone occurred December 27, 2008 to January 7, 2009 beneath northern Yellowstone Lake, Wyoming (Farrell et al., 2009). This sequence consisted of over 1000 earthquakes, 21 of which had magnitudes greater than 3.0. The area of activity migrated progressively north at about ~1000 m/day. Also earthquakes nucleated from as deep as ~10 km and shallowed significantly to 4 km at the north end of the sequence. The largest event had a magnitude of 4.0 and a moment tensor solution that revealed ~50% of the radiated energy as an explosion source with east-west expansion. We particularly note that this unusual earthquake source mechanism is strikingly similar to that of a M 3.3, November 2007, event near the southern caldera boundary that Taira et al. (in press) modeled as a dominantly explosive source earthquake. GPS vectors from nearby stations also suggest east-west expansion of the surface motions. Shortly after the swarm ended on January 7th, a small swarm occurred ~12 km to the north and may have been triggered by the Yellowstone Lake swarm.

Earthquakes in Yellowstone have been routinely monitored since 1973 by permanent and temporary deployments of seismic stations operated by the U.S. Geological Survey (USGS), and the University of Utah Seismic Stations (UUSS) (Smith et al., 1977; Doser and Smith, 1983). This deployment has provided the complete earthquake data set that was used for this study. The seismograph station characteristics and locations of the Yellowstone seismic network are summarized by Husen and Smith (2004).

3. Implications of *b*-value distributions from previous studies

The frequency–magnitude distribution (Ishimoto and Iida, 1939; Gutenberg and Richter, 1944) derives from the power-law relationship between the frequency of occurrence and the magnitude of earthquakes:

$$\log N = a - bM, \quad (2)$$

where N is the cumulative number of earthquakes having magnitudes larger than M , and a and b are constants. It has been shown in laboratory studies, mines, and numerical simulations that the slope of the frequency–magnitude distribution curve, or *b*-value, depends on stress conditions.

Statistically significant variations of *b*-values have been measured in laboratory experiments, mines and various tectonic and volcanic regimes such as subducting slabs, near magma chambers, along fault zones, and in aftershock zones (see for example Wiemer and Wyss, 2002). Seismologists consider that various factors influence *b*-values: (1) increased material heterogeneity, such as a large number of randomly oriented cracks may increase *b*-values (Mogi, 1962); (2) spatial and temporal changes in applied shear stress (Scholz, 1968; Urbancic et al., 1992; Schorlemmer et al., 2004; Schorlemmer and Wiemer, 2005; Schorlemmer et al., 2005) or effective stress (Wyss, 1973) can decrease *b*-values; and (3) an increase in the thermal gradient may increase *b*-values (Warren and Latham, 1970).

In tectonic areas, the *b*-value averages about 1.0 (Frolich and Davis, 1993). In contrast, volcanic areas are characterized by *b*-values greater or less than 1.0 with values as high as 3.0 (McNutt, 2005). Wiemer and Benoit (1996) used a dense spatial grid to study *b*-values at subduction zones. These studies were later extended to volcanic areas. All the aforementioned criteria that favor high *b*-values are found in volcanic areas, such as high heterogeneity due to layering of lava flows and ash, the presence of cooling cracks, dikes and sills, and high thermal gradients. Moreover, because of the dynamic nature of volcanic areas, *b*-values tend to change with changing stress conditions through both time and space.

Seismicity associated with volcanic settings have been studied using *b*-values at several volcanoes including Mt St. Helens and Mt. Spurr, Alaska (Wiemer and McNutt, 1997), Off-Ito volcano, Japan (Wyss et al., 1997), Long Valley Caldera and Mammoth Mountain, California (Wiemer et al., 1998), Soufriere Hills, Montserrat (Power et al., 1998), Mt. Etna, Italy (Murru et al., 1999), Katmai, Alaska (Jolly and McNutt, 1999), Mt. Redoubt, Alaska (Wiemer and Wyss, 2000), Kilauea, Hawaii (Wyss et al., 2001), and Mt. Pinatubo, Philippines (Sanchez et al., 2004). These volcanoes have shown high spatial variability of *b*, with regions of normal *b* (1.0) adjacent to regions with anomalously high *b* (up to 3.0). Most studies have found that in general, *b* is high at depths of 7–10 km where the earthquakes are adjacent to inferred magma bodies. However, some studies also show significant high *b* anomalies at depths of 3–4 km. This is the approximate depth at which magma with 4 wt.% gas starts to exsolve gas, and further, is near the depth at which open cracks may exist in the host rock (McNutt, 2005).

b-values have also been used to infer the state of stress on active faults (Scholz, 1968; Wyss, 1973; Urbancic et al., 1992; Schorlemmer et al., 2004; Schorlemmer and Wiemer, 2005; Schorlemmer et al., 2005).

Schorlemmer et al. (2005) show that there is a general inverse relationship between differential stress and the *b*-value and later conclude that the *b*-value can therefore be interpreted as a 'stressmeter' in the Earth's crust. This idea is supported by the magnitude 6.0 Parkfield, California, event in 2004, which almost exclusively ruptured areas of the San Andreas Fault previously mapped as regions of low *b*-values (Wiemer and Wyss, 1997; Schorlemmer and Wiemer, 2005).

4. Swarm identification

4.1. Method

There are three different types of earthquake sequences (Mogi, 1963): (I) a mainshock followed by a number of aftershocks of decreasing magnitude and frequency (Fig. 3A); (II) a slow build up of seismicity (foreshocks) leading to a type I sequence (Fig. 3B); and (III) a gradual increase and decay of seismicity in time without a distinct mainshock (Fig. 3C) (also see Sykes, 1970). Type III sequences are also known as earthquake swarms and are common in volcanic areas or other remarkably fractured regions or areas where there is a concentrated application of stress such as from intruding magma (Mogi, 1963).

Earthquake sequence I typically occurs in homogeneous material with a uniform external stress. Sequence II tends to occur in material that is heterogeneous to some degree, or a moderate fracture density, with a non-uniform external stress. Sequence III or swarms, occur in material that is extremely heterogeneous, or have high fracture density, with a very concentrated external stress (Mogi, 1963) (Fig. 3).

Various algorithms are available to detect foreshock, mainshock, and aftershock sequences (Reasenberg, 1985; Youngs et al., 1987), but there are few algorithms written to detect earthquake swarms (Waite, 1999). In this study, Reasenberg's (1985) code was first used to identify swarms in the Yellowstone region. However this approach identified events that were clearly not related temporally into a swarm. For example, events up to 5 years apart were classified as members of the same swarm simply because of their spatial relationship.

To identify swarms in the Yellowstone catalog, an algorithm designed by Waite (1999) was used. This algorithm specifies swarms based on the inter-event times and distances based on the swarm definition of Mogi (1963). A swarm is defined if the following criteria are met: (i) the maximum of the daily number of events in the sequence (N_d) is greater than twice the square root of the swarm duration in days (T):

$$N_d > 2\sqrt{T} \quad (3)$$

and (ii) the total number of earthquakes in a sequence E_T is at least 10. Swarms were identified using an E_T value of 10, 30, and 50 to see which criteria best identified both large and small swarms.

4.2. Results

Employing algorithms used to identify foreshock–mainshock–aftershock sequences (Reasenberg, 1985) showed that most earthquake sequences do not follow this pattern because the seismicity in Yellowstone is dominated by swarms during the time period of 1984–2006. Numerous combinations of inter-event times (from 0.5 to 5 days) and distance values (from 2 to 15 km) were included in the swarm identification algorithm of Waite (1999). In addition, various definitions of minimum number of earthquakes that constituted a swarm, from 5 to 50 were examined. The combination of an inter-event time of 2 days and a distance of 5 km most reliably identified both large and small swarms in the Yellowstone region and the results are summarized in Table 1 (Results from the 10 and 50-minimum definition of a swarm can be seen in Fig. S1A and S1B respectively).

Sixty-nine individual swarms were identified (Fig. 4, Table S1) using the criteria in which a swarm must have at least 30 events (30-minimum). These swarms varied in duration from 1 to 46 days, total

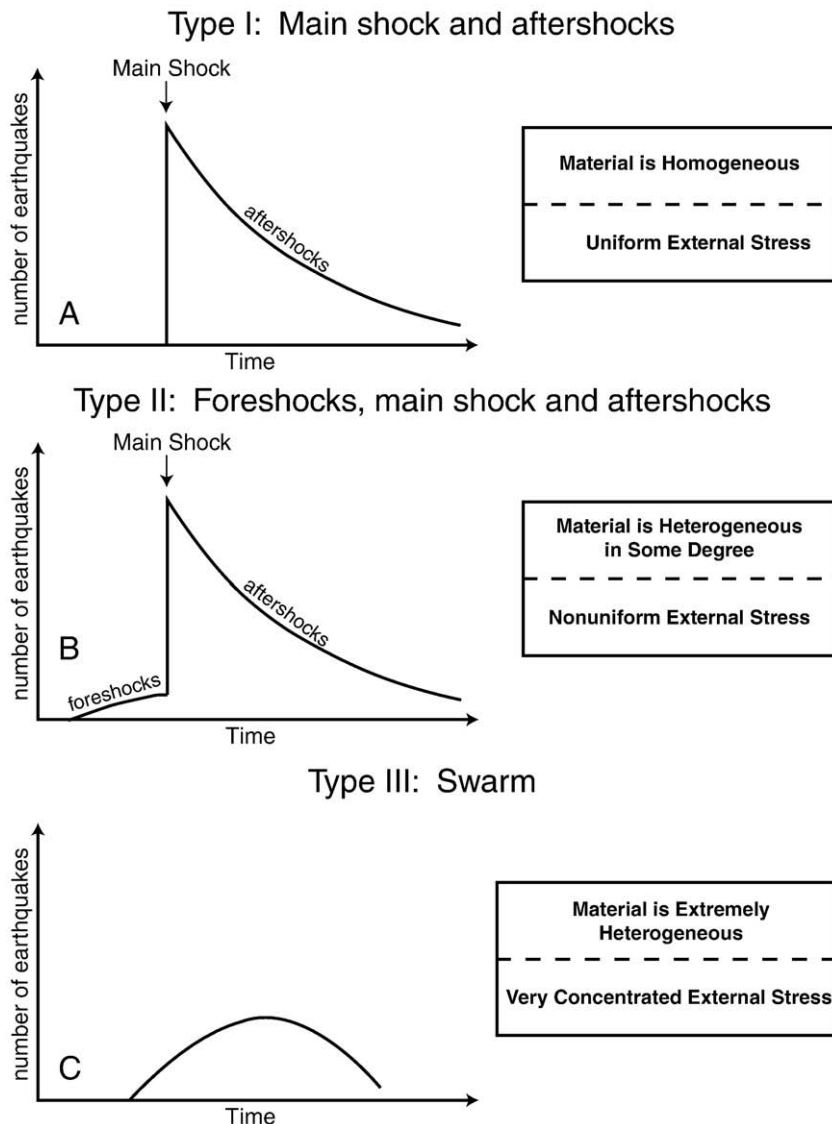


Fig. 3. Generalized plots of number of earthquakes vs. time for the three types of earthquake sequences after [Mogi \(1963\)](#).

number of events from 30 to 722, and maximum number of events per day from 9 to 295. The average number of events per swarm for all 69 swarms is 129.3. The total number of events for all 69 swarms is 8924, which is 39.0% of the original 23,054 events. Magnitudes of swarm events range from $-1.19 \leq M_c \leq 4.82$ with 99.9% of the swarm events having magnitudes less than or equal to $M_c = 4.0$; 99.7% having $M_c \leq 3.0$; 96.2% having $M_c \leq 2.0$; and 68.0% having $M_c \leq 1.0$. Fifty-four (78.3%) of the 69 swarms are located in the region just north and northwest of the Yellowstone caldera. Fourteen (20.3%) are located within or on the boundary of the 0.64 Ma caldera. One (1.4%) is located outside the 0.64 Ma caldera to the east or south.

[Waite \(1999\)](#) identified 72 swarms in the Yellowstone region for the period 1973 to 1997. Although we have identified many of the same swarms in this study, comparisons cannot be made in some cases because [Waite \(1999\)](#) used the original, non-relocated, earthquake catalog to identify swarms. Here, only the quality A, B, and C earthquakes of the relocated catalog of [Husen and Smith \(2004\)](#) were used and many additional earthquakes were eliminated in the relocation process. The relocated catalog was used in this study because in order to calculate b -values, high quality earthquake locations are important both for identifying swarms and for accurately mapping the spatial changes of b -values.

[Waite \(1999\)](#) identified 3156 earthquakes in the autumn 1985 swarm. However, using the relocated catalog, the swarm was found to consist of only 462 earthquakes. From 1995 to 2006 the swarms identified in this study become more similar to the swarms identified by [Waite \(1999\)](#) in both the number of swarms and the total number of earthquakes in each swarm. This is because the seismic network upgrades improved the quality of the earthquake locations so that more earthquakes made it through the relocation process.

For example, [Waite \(1999\)](#) identified a swarm on the northwest Yellowstone caldera boundary, near Madison Junction starting in June of 1995 that consists of 581 earthquakes. That same swarm calculated here was actually composed of four smaller swarms. The total number of earthquakes in these four swarms is 567. The reason that the swarm sequence was divided into four different swarms here is because a more refined search radius of 5 km was used in this study while [Waite \(1999\)](#) used a search radius of 15 km.

Although direct comparisons to results from [Waite \(1999\)](#) cannot be made with individual swarms, the patterns of swarms can be compared. The high percentage of swarms located in the area north and northwest of the Yellowstone caldera (69%, 78.3%, and 79.2% for the 10-minimum, 30-minimum, and 50-minimum definitions, respectively) is comparable to the results of [Waite \(1999\)](#). This suggests

Table 1

Summary of de-swarming results using various definitions of a swarm.

Swarm definition	# of swarms	Duration (days)	# of events	Max # of events/day	Avg. # of events/swarm	Total # of events	% of original catalog
10-min	239	1 to 46	10 to 722	2 to 295	49.1	11,740	50.9
30-min	69	1 to 46	30 to 722	9 to 295	129.3	8924	39.0
50-min	48	2 to 46	50 to 722	11 to 295	168.9	8109	35.2
Swarm definition	Magnitude (M_c) range	% of events with $M_c \leq 4.0$	% of events with $M_c \leq 3.0$	% of events with $M_c \leq 2.0$	% of events with $M_c \leq 1.0$	% of swarms located north of the caldera	% of swarms located in the caldera
10-min	−1.19 to 4.82	99.98	99.70	95.49	65.03	69.0	29.3
30-min	−1.19 to 4.82	99.90	99.70	96.20	68.00	78.3	20.3
50-min	−1.19 to 4.19	99.99	99.77	96.20	67.30	79.2	18.8

that the crust in that area is highly fractured and heterogeneous. The abrupt change in topography may suggest that the boundary of the 2.05-Ma caldera (caldera I) is located in this area (dashed line in Fig. 2). Swarm epicenters in this area also tend to align in a more east-west trend, which is what would be expected from the orientation of the edge of caldera I. Another explanation for the high rate of seismicity in this region is the increased stress resulting from the 1959 M7.5 Hebgen Lake, MT earthquake (Chang and Smith, 2002).

Swarm earthquake epicenters within and adjacent to the 0.64-Ma caldera are generally aligned in a north-northwest direction. This alignment is sub-parallel to alignments of post-caldera volcanic vents and Quaternary faults (Fig. 1) and implies that these events could have occurred on preexisting zones of weakness such as buried but still active Quaternary faults (Christiansen, 1984).

5. Calculating b -values

5.1. Method

Wiemer and Wyss (2000) suggest that a careful estimate of the spatial and temporal homogeneity of the magnitude of completeness (M_{COMP}) is required before deviations from a power law behavior for small magnitudes can be made. Therefore, M_{COMP} , which is the minimum magnitude in which the catalog is complete, was calculated for the Yellowstone earthquake catalog. It is well known that M_{COMP} can decrease with time in most earthquake datasets because the number of seismographs increases and the methods of analysis improve (Wiemer and Wyss, 2000). M_{COMP} was calculated using the EMR method described by Woessner and Wiemer (2005).

The b -values determined in this study were calculated using the ZMAP algorithm (Wiemer, 2001). Maximum-likelihood b -values were computed using the following equation (Utsu, 1965; Aki, 1965; Bender, 1983):

$$b = \frac{1}{\bar{M} - M_{min}} \log e, \quad (4)$$

where \bar{M} is the mean magnitude and M_{min} the minimum magnitude of the given sample. The sample is considered complete down to the minimum magnitude M_{min} . The magnitude of completeness (M_{comp}) has to be corrected by $\Delta M/2$ to compensate the bias of rounded magnitudes to the nearest ΔM bin, thus $M_{min} = M_{comp} - \Delta M/2$ (Utsu, 1965; Guo and Ogata, 1997). The confidence limit of this b -value estimation is given by (Shi and Bolt, 1982):

$$\sigma(b) = 2.30b^2 \sqrt{\sum_{i=1}^n (M_i - \bar{M})^2 / n(n-1)} \quad (5)$$

where n is the total number of events of the given sample.

For volumetric sampling of earthquakes, we employed cylindrical volumes centered at nodes spaced at 0.01° (latitude) \times 0.01° (longitude)

($\sim 1.1 \text{ km} \times \sim 0.8 \text{ km}$) with varying radii for the cylinders. For cross-sections, sampling is done on a $0.5 \text{ km} \times 0.5 \text{ km}$ grid with varying radii. For each node a minimum number of events, N_{min} , with $M \geq M_{comp}$ is required in order to determine a reliable b -value. For samples that contain less than N_{min} events, a b -value is not calculated. N_{min} is set to 50 in this study because below this value the uncertainty in the b -value increases rapidly (Schorlemmer et al., 2004). Radii were varied from 3 to 10 km and results were compared. The radius that produced robust results with the greatest spatial extent was chosen.

The b -value distribution for each different criterion for removing swarms and with the full catalog was mapped and compared to identify the influence of removing swarms. To compare b -values for different criteria for removing swarms and with the full catalog, b -values are spatially mapped for both types of data. If in both instances, the sample size is greater or equal to N_{min} and thus a b -value can be computed, the probability P_b of the hypothesis that the b -values of the two catalogs are coming from the same population is computed. This probability value is derived from the Akaike Information Criterion (AIC) (Akaike, 1974). Comparing the ΔAIC_0 for both catalogs having the same b -value b_0 and the ΔAIC_{12} for both catalogs having two different b -values b_1 and b_2 leads to the difference ΔAIC of these two AIC scores as given by Utsu (1992):

$$\begin{aligned} \Delta \text{AIC} = & -2(N_1 + N_2) \ln(N_1 + N_2) + 2N_1 \ln\left(N_1 + \frac{N_2 b_1}{b_2}\right) \\ & + 2N_2 \ln\left(\frac{N_1 b_2}{b_1} + N_2\right) - 2 \end{aligned} \quad (6)$$

Where N_1 and N_2 are the number of earthquakes in each group and b_1 and b_2 are the b -value of each group. The probability P_b that the b -values are not different is given by:

$$P_b = e^{[-(\Delta \text{AIC}/2)-2]} \quad (7)$$

Using the criteria from Utsu (1999), the difference in b -values is considered not significant if $\Delta \text{AIC} < 2$. If $\Delta \text{AIC} > 2$, the difference is significant. $\Delta \text{AIC} = 2$ corresponds to $P_b \approx 0.05$. The difference is considered highly significant if $\Delta \text{AIC} > 5$, with a corresponding probability of $P_b \approx 0.01$. Applying the logarithm leads to log-probabilities of $\log P_b \leq -1.3$ for significantly different b -values and $\log P_b \leq -1.9$ for highly significant differences in b -values (Schorlemmer et al., 2004; Schorlemmer et al., 2005).

5.2. Threshold of magnitude completeness

The seismicity rate for quality A, B, and C earthquakes in the Yellowstone region increased from ~ 200 earthquakes per year before 1995 to ~ 1500 earthquakes per year after 1995 (Fig. 5). However, this change in seismicity rate is due to upgrades and expansion of the

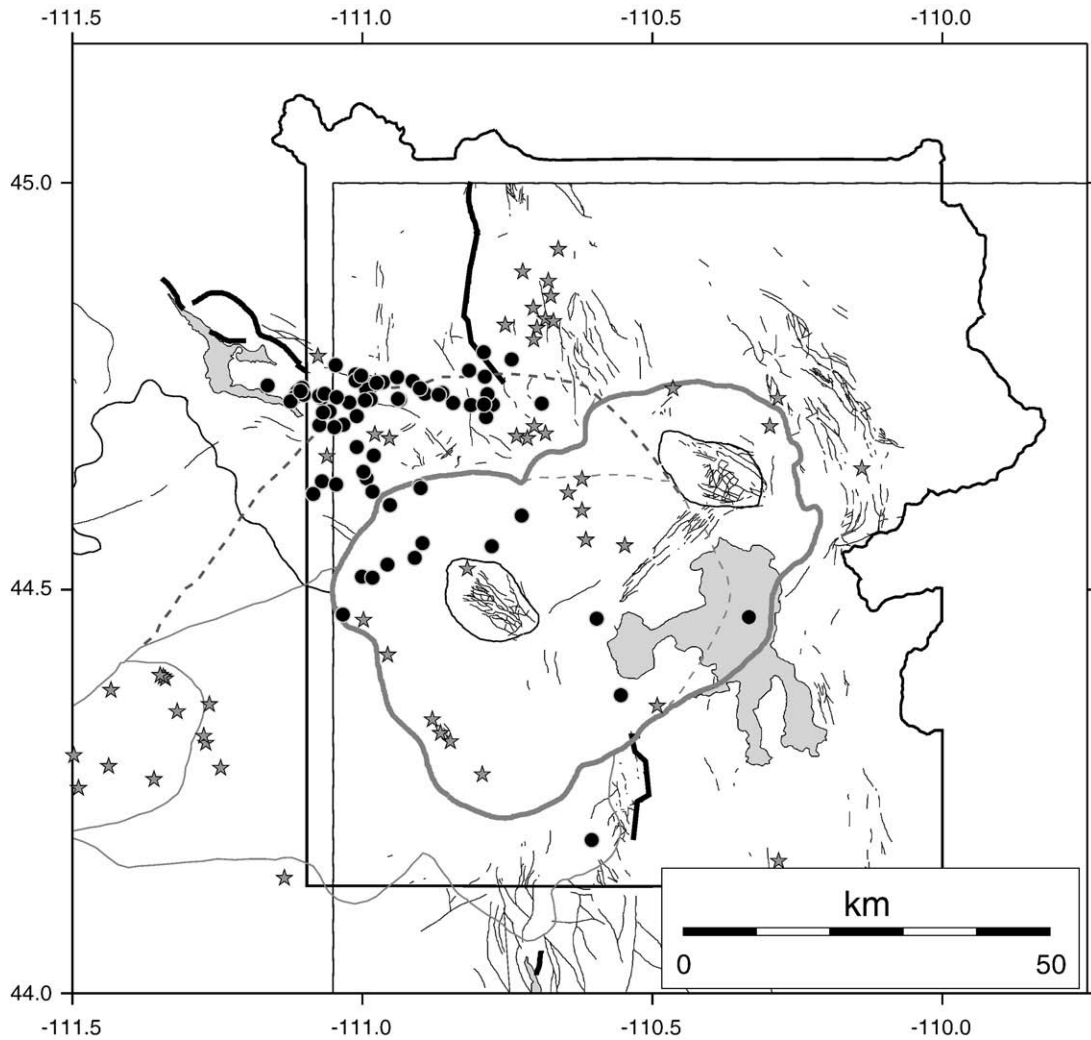


Fig. 4. Swarm locations identified while using the 30-minimum definition of a swarm used in this study. Mean locations for the 69 swarms are shown by black dots. Post-caldera volcanic vents are shown as gray stars (Christiansen, 2001). The 0.64-Ma caldera is outlined as a thick gray line and the 1.3-Ma and 2.05-Ma caldera boundaries are outlined as thin gray lines, with the possible northern extent of the 2.05-Ma caldera shown with a dashed gray line. Quaternary faults after Christiansen (2001) are shown as thin black lines. Major Quaternary faults are shown as thick black lines.

seismic network. Beginning in 1995, three-component short-period and broadband seismometers were added to the network. Therefore the catalog data were divided into two time periods, 1984–1994 and 1995–2006. Also, due to the higher density of both seismometers and earthquakes, events in the area that extends from Hebgen Lake east to the northern caldera boundary near Norris Junction was separated from the rest of the catalog (Fig. 6). Fig. 6 shows the magnitude of completeness values calculated for the various spatial and temporal areas. The highest value of M_{COMP} was selected ($M_{\text{COMP}} = 1.5$ based on the time period 1984–1994 for the remaining region), and the catalog was cut there and the remaining events were then used to calculate b -values to ensure that M_{COMP} is consistent throughout the time period of the catalog as well as throughout the entire area. Fig. 7 shows the number of earthquakes remaining to calculate b -values after a) de-swarming, b) removing triggered events from the 2002 M7.9 Denali fault earthquake, and c) cutting the catalog at $M_{\text{comp}} = 1.5$.

5.3. b -value results

Epicenter locations used to calculate b -values for the various swarm definitions are plotted in Fig. 7. As expected, as the minimum number of events that constitute a swarm is increased, more events are left in the

catalog to calculate b -values. To investigate the influence of using different swarm definitions on the stability of the b -value results we computed b -values using the different data sets, including the complete, non-de-swarmed catalog. The resulting spatial distribution of b -values in Yellowstone shows areas of high and low b -values and areas of normal crustal values ($b \approx 1.0$) (Fig. 8). A constant 10 km radius was chosen to calculate the b -values because this radius allowed the maximum coverage while still showing details of the areas with both high and low b -values.

The probability P_b of the possibility that the b -values of the two catalogs are from the same population is computed in order to quantitatively identify the differences between the b -value maps for the three different de-swarmed catalogs as well as the non-de-swarmed catalog (Eq. (7)). In Fig. 9, b -values are significantly different when $\log P_b \leq -1.3$ and the b -values show highly significant differences for $\log P_b \leq -1.9$ (Schorlemmer et al., 2004; Schorlemmer et al., 2005).

Statistically, there is little difference between the b -values using the de-swarmed catalogs from the 10-minimum events and 30-minimum events definition of a swarm (Fig. 9A). The 30-minimum catalog is preferred over the catalog from the 10-minimum definition of a swarm due to the fact that using the catalog from the 30-minimum definition of a swarm provides greater spatial coverage for mapping b -values.

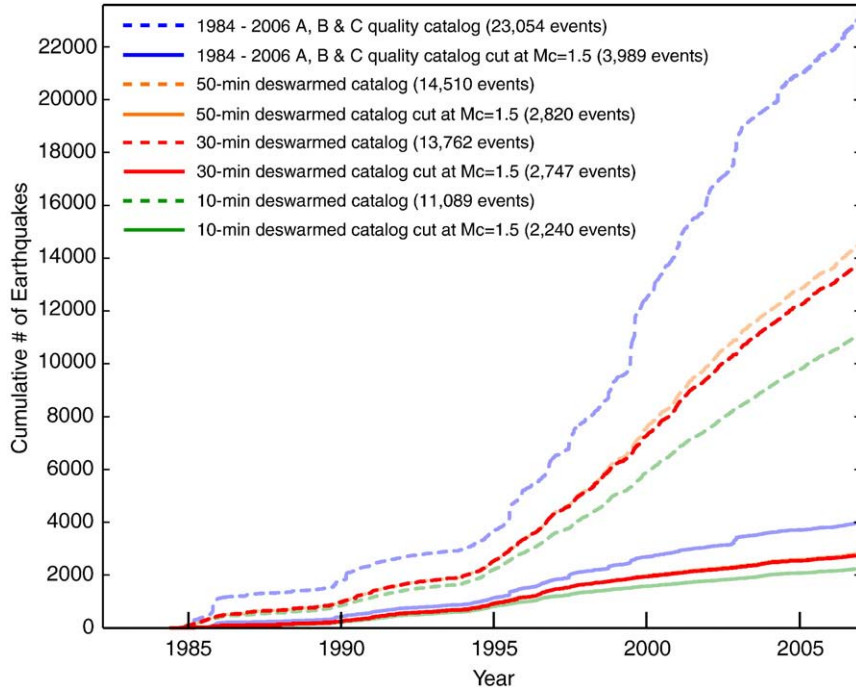


Fig. 5. Cumulative number of earthquakes vs. time for the various Yellowstone earthquake catalogs used to calculate b -values. Blue dashed line shows the original catalog consisting of A, B, and C quality events from 1984 to 2006. Dashed lines represent the de-swarmed catalogs using the various definitions of a swarm. Solid blue line represents the quality A, B, and C events from 1984 to 2006 cut at $M_{COMP} = 1.5$. Remaining solid lines represent the de-swarmed catalogs cut at $M_{COMP} = 1.5$.

When comparing the b -values from the 30-minimum dataset and the 50-minimum dataset, there are slight differences in the center of the Yellowstone caldera. Overall only 0.24% of the nodes are different between the two datasets (Fig. 9B). The reason for the differences is a swarm that occurred in August of 1999 (Swarm 30 in Table S1). This swarm consisted of 35 earthquakes so it is only identified and subsequently removed by the algorithm with the 30-minimum definition of a swarm. This swarm contained an earthquake of $M_C = 4.82$, which introduced a significant difference between the 30-minimum and 50-minimum models by biasing the b -value calculations (Fig. 10). Because this swarm could be considered an outlier, we prefer to remove it from the catalog by using the dataset from the 30-minimum swarm definition.

Only data at 0.18% of the sampling interval are significantly different (Fig. 9C) when comparing the b -values from the 30-minimum dataset with the b -values from the original, unsorted dataset. Some of these differences are due to the same swarm event that was just discussed. Just to the north of the Yellowstone caldera another area shows significantly different b -values. The differences here are attributed to five events ranging from $3.0 \leq M_C \leq 3.8$. These five earthquakes were identified in two swarms and were removed in the 30-minimum dataset. Because they all occurred in the same area, they all influenced the b -value calculation for the original catalog. The unfiltered catalog was discarded and the 30-minimum dataset was chosen as the most stable and best catalog to use when interpreting b -values because the b -value is influenced heavily by just these five events.

There are three areas of relatively high b -values for the 30-minimum event catalog (Fig. 11). The area with the highest b -values is associated with earthquakes of the Mallard Lake resurgent dome (MLD) where b -values are as high as 1.5 ± 0.05 . This area of high b -values extends north from the MLD to Madison Junction. A secondary area with high b -values is located near Norris Geyser Basin (NGB) and extends north along the Norris–Mammoth Corridor and east to the northern boundary of the Yellowstone caldera. The Gallatin fault bounds this area of elevated b -values to the west. Here we see values of b up to 1.3 ± 0.05 . The third

area where we see elevated b -values is in the Hebgen Lake area just west of the Yellowstone National Park border. This area is also the site of the $M = 7.5$ Hebgen Lake earthquake in 1959. The highest b -value in the Hebgen Lake area was 1.3 ± 0.1 just to the northeast of the Red Canyon fault.

Two areas had relatively low b -values. The first is east of the Sour Creek Resurgent Dome (SCD) on the park border, with b -values as low as 0.5 ± 0.1 . This is an area that has experienced persistent seismic activity throughout the entire time span of Yellowstone earthquake recording. The second area of low b -values is located at the southern portion of the Yellowstone caldera near the Mt. Sheridan fault (MSF) and near the northern extent of the Teton fault. In this area b -values are as low as 0.6 ± 0.1 .

We have determined the errors in our calculations to assess the validity of our calculations (Fig. 12). The majority of the errors in b -values are less than 0.1. The largest errors in b (~ 0.15) are located on the eastern side of the 0.64-Ma caldera. These larger errors are due to the inclusion of a $M_C = 4.8$ earthquake that occurred in 1999. The difference in the frequency–magnitude distribution due to this single event can also be seen in Fig. 10. The lowest errors (< 0.05) occur in the area north of the 0.64-Ma caldera where the highest concentration of epicenters is located.

The depth distribution of b -values as well as the temporal changes in b -values was also examined, but because of our limited range in epicenter depths, our sampling radius of 5 km was too large to image differences in the b -value with depth. In addition, after filtering, there were too few earthquakes to adequately detect changes in b -values over time.

6. Discussion

6.1. Swarm identification

Using the definition that a swarm had to contain at least 30 events, $\sim 39\%$ of the recorded earthquakes in the Yellowstone region are associated with swarms. Of the 69 swarms identified, 54 (78.3%) are located in the region north and northwest of the Yellowstone caldera

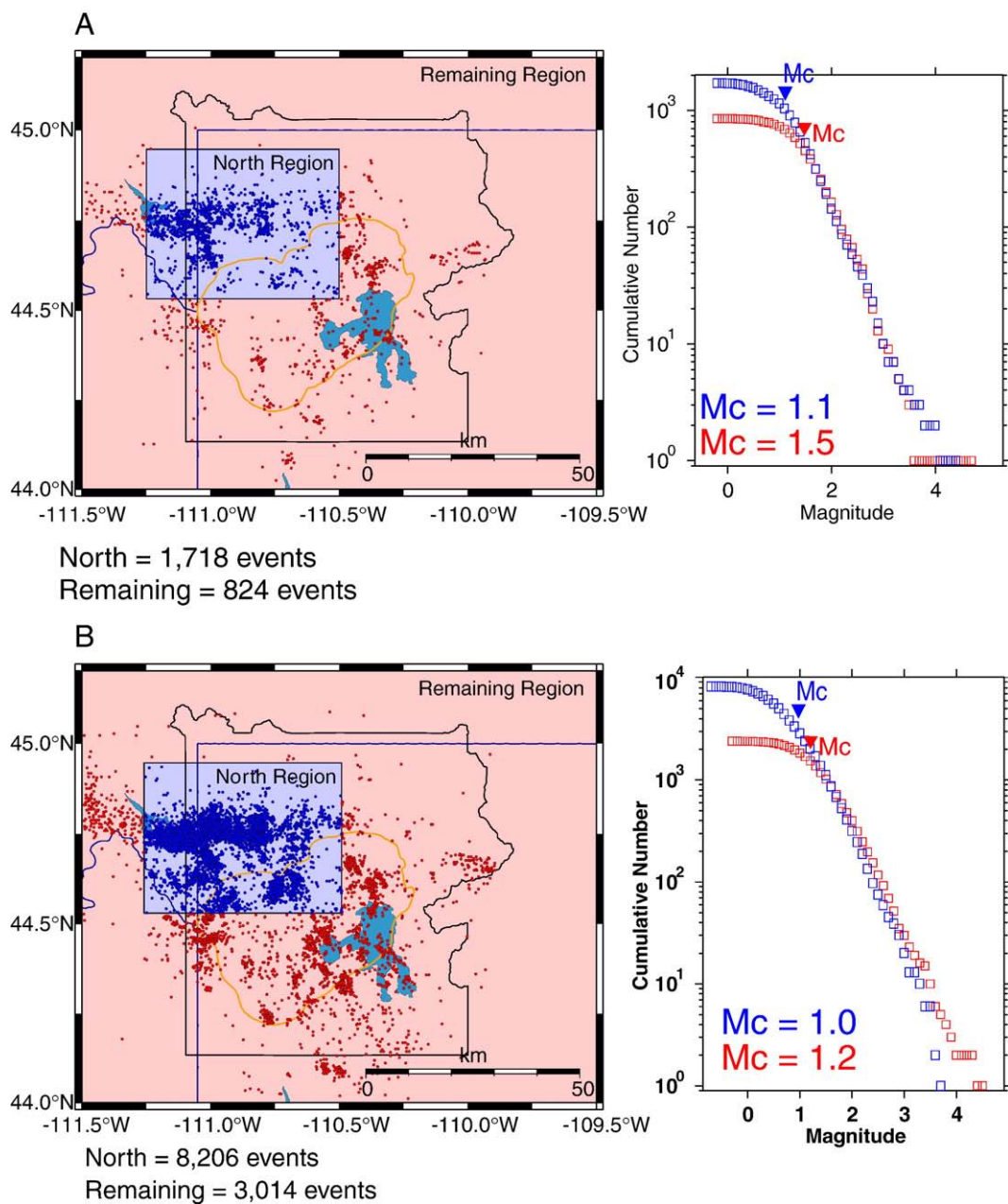


Fig. 6. Threshold of earthquake completeness (M_{COMP}) calculations for the 30-minimum de-swarmed catalog. (A) shows M_{COMP} values for the years 1984–1994 and (B) shows M_{COMP} values for the years 1995–2006. Blue color represents the north region and red color represents the remaining region.

while 14 (20.3%) are located within or at the Yellowstone caldera boundary (Fig. 4).

Because a high number of swarms were identified in the east–west band of seismicity extending from the Hebgen Lake fault to the Norris Geyser Basin, we interpret the seismogenic upper crust here to be highly fractured, with a large number of small magnitude earthquakes occurring on numerous small fractures. This interpretation is based on the concentration of earthquake swarms that are often associated with volcanic features or other fractured regions where there is a concentrated application of stress such as intruding magma (Mogi, 1963). There is also an abrupt change in the topography in this region and the east–west alignment of swarm epicenters here indicates that this is the location of the northern rim of the 2.05-Ma caldera (caldera I, dotted line in Fig. 1), which is about 15 km north of the mapped Yellowstone caldera rim of Christiansen (2001).

Moreover it is considered that the Gallatin Range was once continuous to the south but is now covered beneath young volcanic rocks of the Yellowstone giant silicic eruptions (Christiansen, 2001). During the first catastrophic eruption 2.05 million years ago, the mountain range was destroyed by the explosive caldera-forming eruption and by caldera collapse (Smith and Siegel, 2000). The east–west alignment of swarm epicenters in this area is significant in that the swarms may be occurring on preexisting zones of weakness from the 2.05-Ma caldera eruption.

It also has been shown that Yellowstone swarms can be attributed to the migration of magmatic or hydrothermal fluids (Waite and Smith, 2002). Although these swarms are much smaller in both the number of earthquakes as well as the spatial extent of earthquakes than the 1985 swarm that was examined by Waite and Smith (2002), it is plausible to hypothesize that the associated earthquakes are the

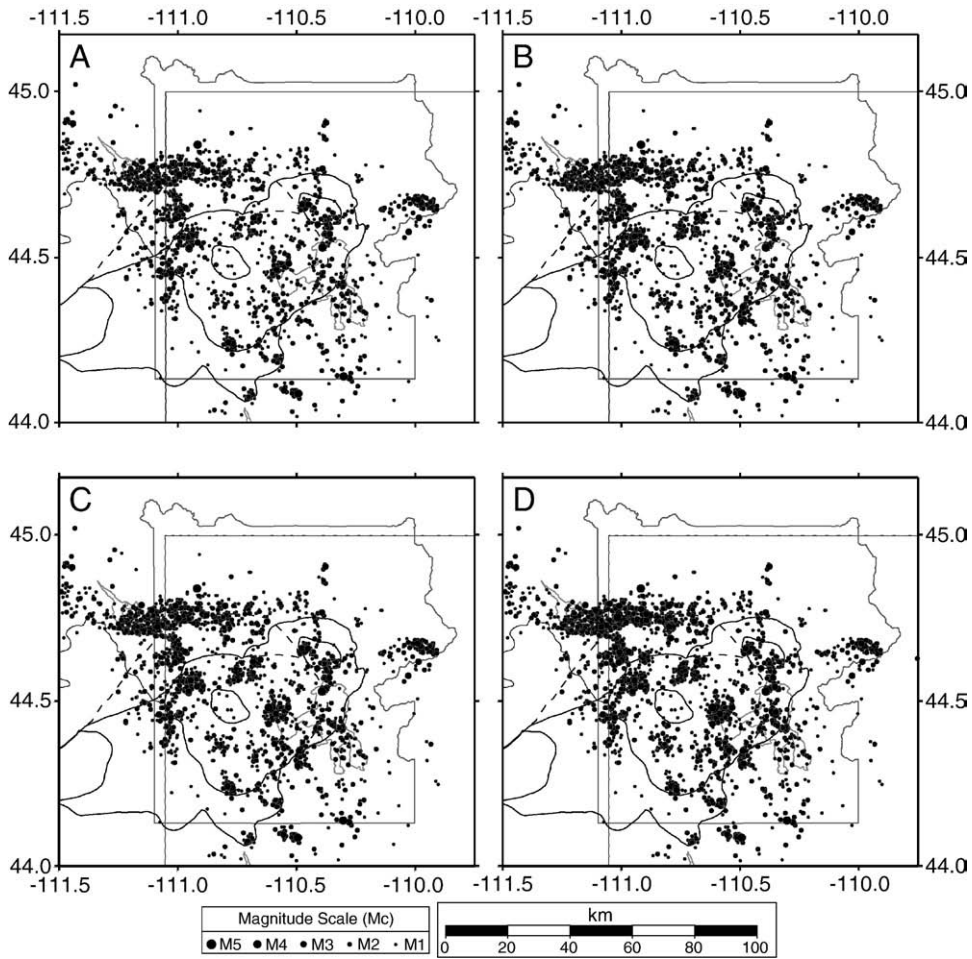


Fig. 7. Earthquakes of the Yellowstone region used to calculate b -values for the various de-swarmed and non-de-swarmed catalogs. A) shows the 2240 epicenters for the 10-minimum de-swarmed catalog, B) shows the 2747 epicenters for the 30-minimum de-swarmed catalog, (C) shows the 2820 epicenters for the 50-minimum de-swarmed catalog, and (D) shows the 3989 epicenters for the non-de-swarmed catalog.

result of a migration of fluids (magmatic and/or hydrothermal) along either pre-existing cracks or propagating dikes.

Hill (1977), for example, suggested a process to explain earthquake swarms: In a series of dikes oriented with their long dimension parallel to the regional greatest principal stress, shear failures occur along oblique fault planes connecting adjacent tips of en echelon or parallel dikes when a critical combination of fluid pressure in the dikes and the difference between σ_1 and σ_3 is reached.

Summarizing other swarm studies, Toda et al. (2002) also suggested that the 2000 Izu Islands, Japan earthquake swarm was caused by a laterally propagating dike intrusion. Waite and Smith (2002) propose that the 1985 swarm in Yellowstone was due to the migration of magmatic or hydrothermal fluids. In particular they state that the most likely scenario for the swarm involves the rupture of a self-sealed hydrothermal layer and subsequent migration of hydrothermal fluid through a preexisting fracture zone out of the Yellowstone caldera. More recently, Vidale et al. (2006) suggested that swarms may be due to non-magmatic sources such as a variable component of background seismicity driven by aseismic slip and fluid pressure variations.

6.2. b -value distribution

We interpret the area of high b -values (up to 1.5 ± 0.05) in the area located near the Mallard Lake resurgent dome (MLD) (Fig. 11) to be influenced by high crustal heterogeneity of the local stress regime, a high thermal gradient and magmatic fluids. This high heterogeneity

of stress causes numerous small cracks in the crust to be oriented in all directions. Under these conditions, the likelihood of large earthquakes occurring is decreased because a rupture terminates when it encounters an existing crack orientated unfavorably for failure. In such a highly fractured crust, many small ruptures would be observed but fewer larger ones, which is what is observed in the frequency-magnitude distribution (Wiemer et al., 1998). The average magnitude of events in this area is ~ 1.5 and corresponds to an average rupture length of about 70 m (Wiemer and McNutt, 1997; Kanamori and Anderson, 1975). Small cracks produce only small earthquakes because of their short source length. This is comparable with results from the Long Valley Caldera in eastern California, which is a similar large silicic volcanic center where Wiemer et al. (1998) found high b -values ($b > 1.5$) in the area near the resurgent dome and interpreted these to be the result of a highly fractured crust (Hill, 1992).

The high thermal gradient in the Yellowstone caldera is considered to be attributed to the presence of magmatic fluids below the surface (Eaton et al., 1975; Fournier, 1989; Husen et al., 2004a). The shallowest earthquakes in the area occur beneath the MLD (Fig. 1) where the depth of 80% of the hypocenters is ~ 5 km (Smith et al., 2009-this volume). This depth is interpreted as the brittle-ductile transition zone with a temperature of ~ 400 °C (Sibson, 1982; Smith and Bruhn, 1984; Fournier, 1999) and gives a thermal gradient of ~ 80 °C/km for the area beneath the Mallard Lake resurgent dome. If the average 80th percentile depth of 8 km inside the 0.64-Ma caldera is used, an average thermal gradient of ~ 50 °C/km is determined.

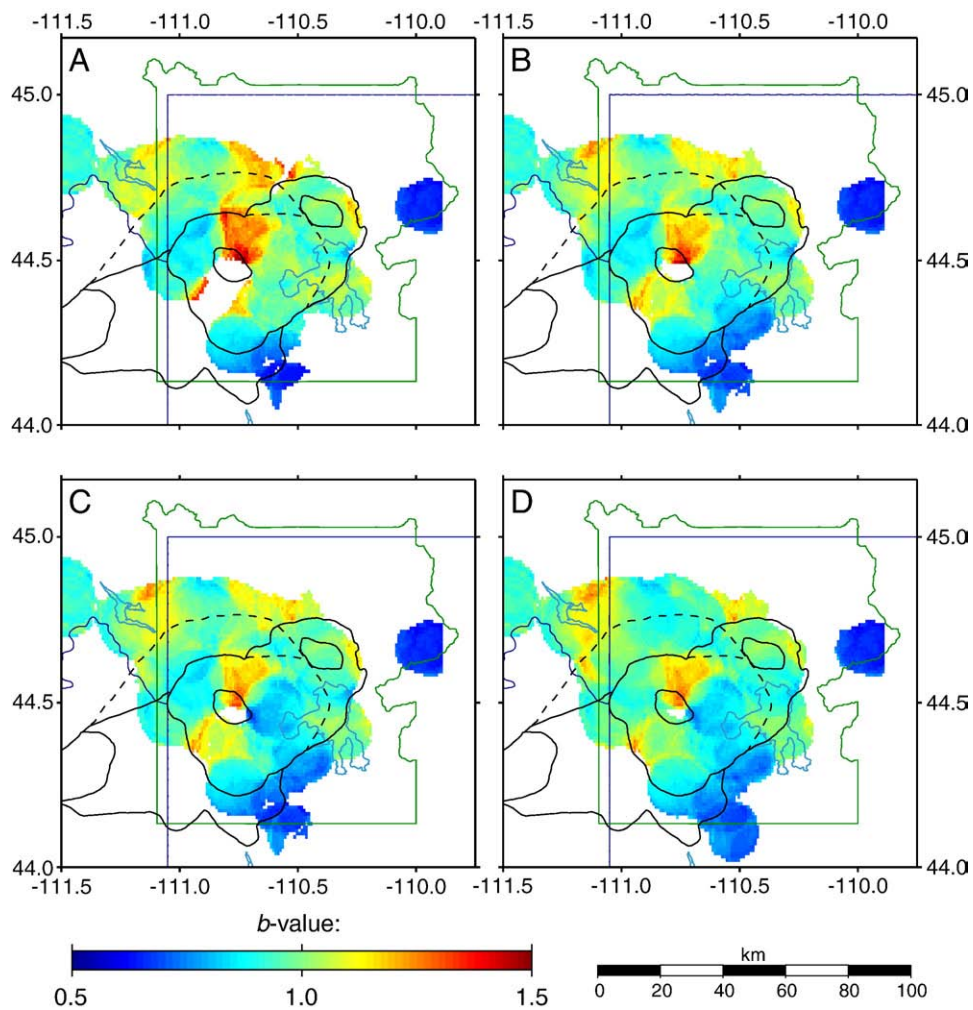


Fig. 8. b -value maps for all the earthquake listings shown in Fig. 7. (A) b -values calculated for the 10-minimum de-swarmed catalog, (B) b -values calculated for the 30-minimum de-swarmed catalog, (C) b -values calculated for the 50-minimum de-swarmed catalog, and (D) b -values calculated for the non-de-swarmed catalog. Red-orange colors indicate high b -values and blue-green colors represent low b -values.

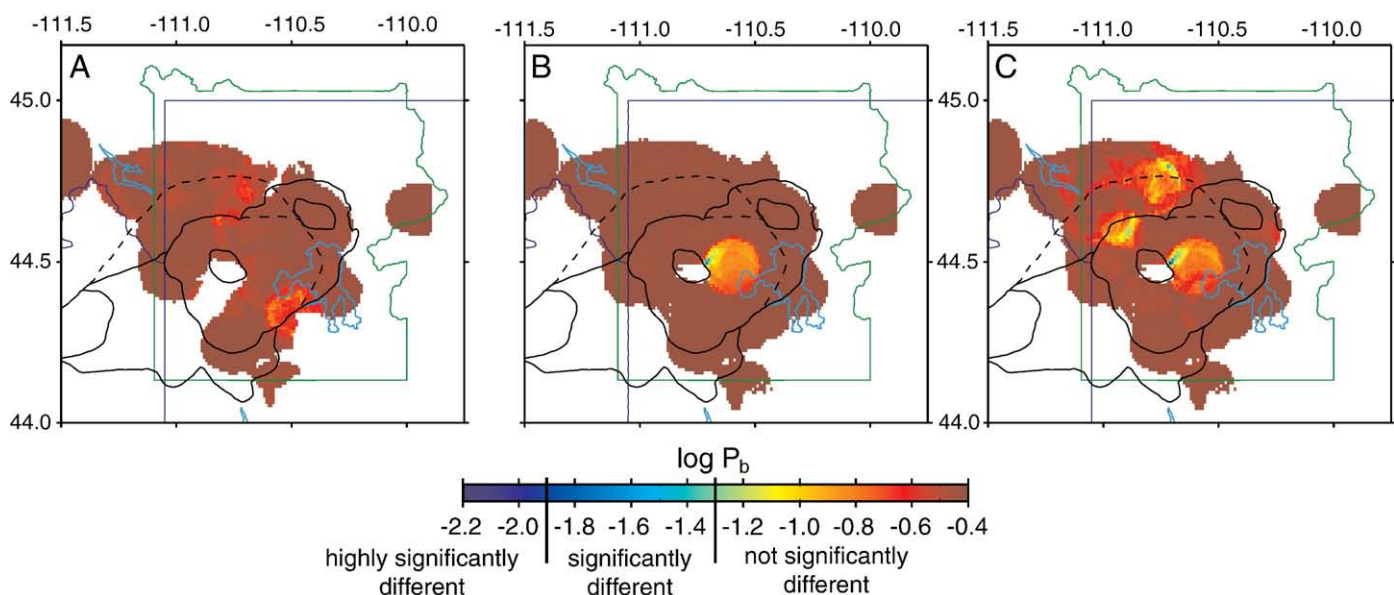


Fig. 9. Utsu Test results (Utsu, 1992) comparing the various b -value maps. (A) 10-minimum vs. 30-minimum, (B) 30-minimum vs. 50-minimum, and (C) 30-minimum vs. non-de-swarmed. Red colors show values that are not significantly different and blue to green colors show values that are statistically different.

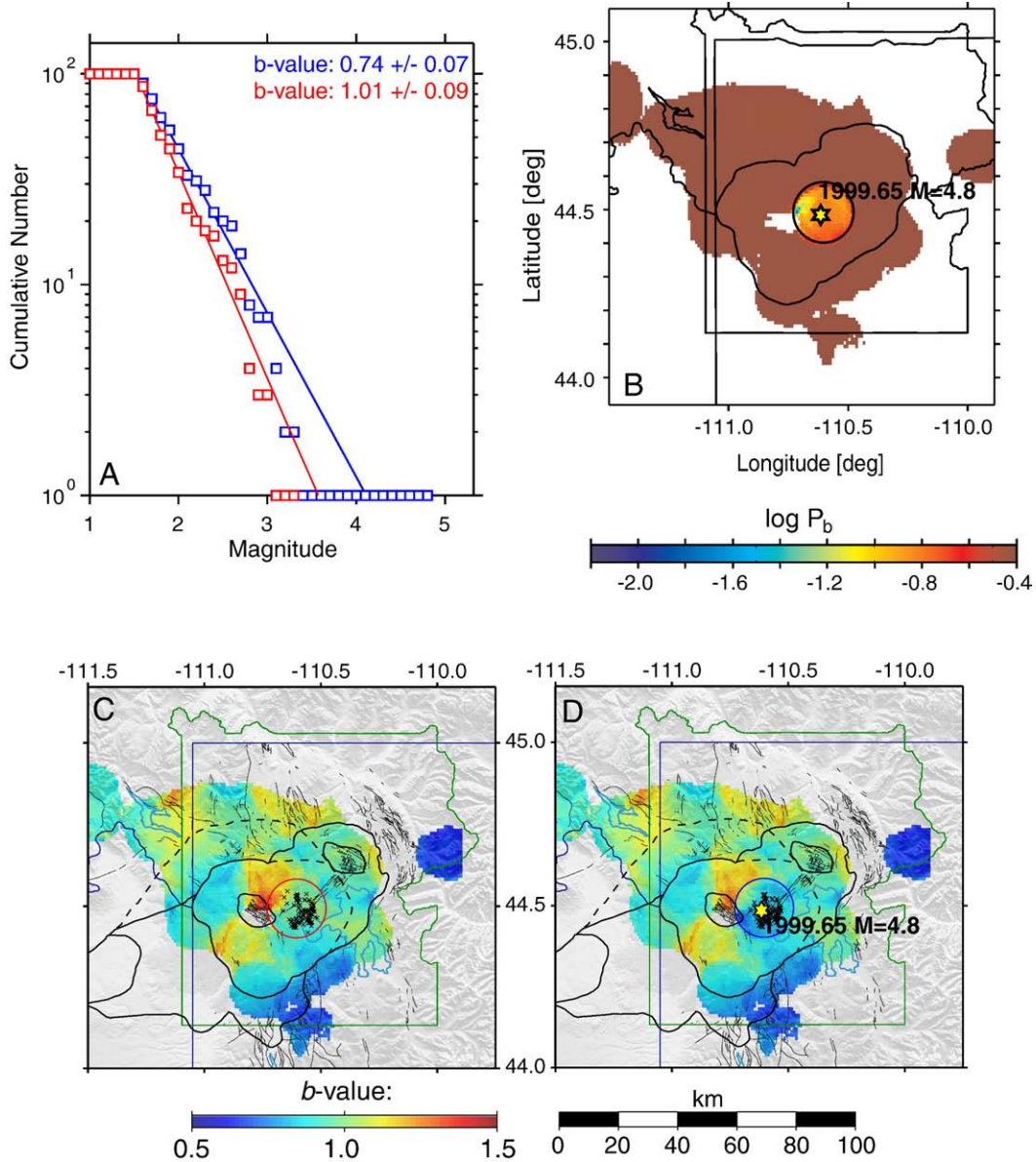


Fig. 10. Frequency–magnitude distribution (FMD) comparison for the 30-minimum b -value map vs. the 50-minimum b -value map. (A) Shows the FMDs for the two samples shown in C and D. Colors match the colors of the sampling radii shown in the circles in C and D. (B) Shows the Utsu test results with significantly different b -values in the central Yellowstone caldera. (C) Shows the b -value distribution with the sampling radius (red) for the 30-minimum de-swarmed catalog. (D) Shows the b -value distribution with the sampling radius (blue) for the 50-minimum de-swarmed catalog.

Smith and Braile (1994) estimated an average thermal gradient for the Yellowstone region of $\sim 45\text{ }^{\circ}\text{C/km}$. This supports the results of Warren and Latham (1970), in which they show that an increase in the thermal gradient causes an increase in b .

The emplacement of magma and the accompanying crustal expansion as suggested by Wicks et al. (2006) and Chang et al. (2007) for the high crustal deformation rates would give rise to factors responsible for high b -value measurements. Mainly high heterogeneity of the crust due to numerous cracks from the increased stress and a high thermal gradient, which is also supported by focal depth distribution. Given that the period of uplift and the period of high b -values overlap in time, these could be the underlying reasons for the high b -values measured in this study.

The area of high b -values of up to 1.3 ± 0.05 north of the Yellowstone caldera rim extending from Norris Geyser Basin may also be a result of magmatic fluids migrating from the Yellowstone caldera

north into the Norris–Mammoth Corridor (Wicks et al., 2006) (Fig. 11). Again, the presence of magma gives rise to the main factors causing higher b -values, mainly high heterogeneity, and high thermal gradient. The presence of partial melt causes higher temperatures. In turn, a zone of relatively lower stress around the area of partial melt is created because the high temperatures reduce the strength of the material which would not allow significant stress buildup. Numerous small cracks would form as the area of partial melt pushed up through the crust as well.

The area of high b -values located near Hebgen Lake exhibiting values up to 1.3 ± 0.1 could also be the result of magma migrating laterally from the Yellowstone caldera (Fig. 11). More likely, high b -values in this area are a reflection of a relatively low stress regime as a result of the 1959 Hebgen Lake earthquake. Chang and Smith (2002) show that the 1959 $M7.5$ Hebgen Lake earthquake caused a decrease in the Coulomb failure stress of about 0.4 MPa (compared to a static-

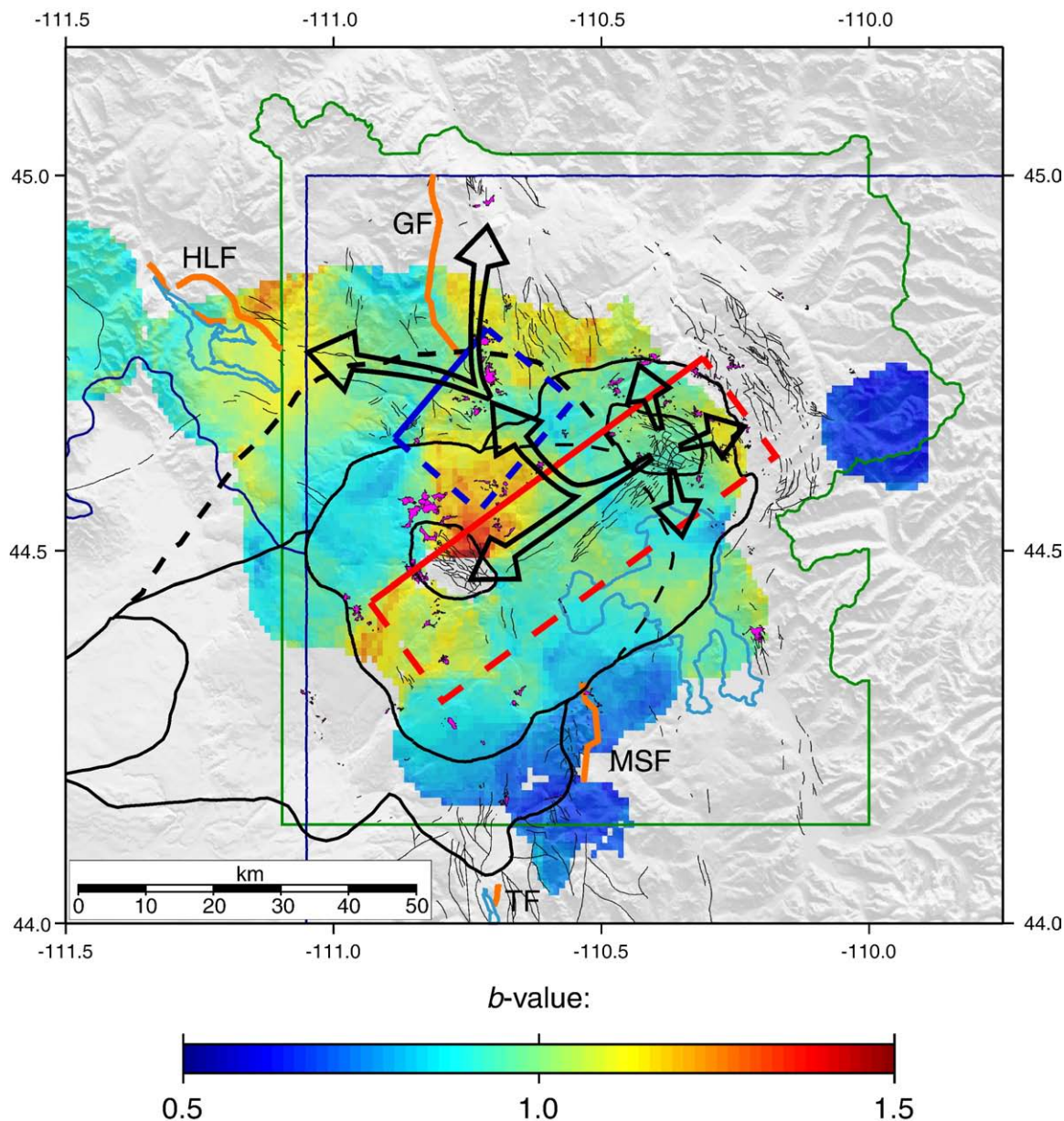


Fig. 11. Spatial *b*-value distribution for the 30-minimum Yellowstone de-swarmed catalog. Red to orange colors represent high *b*-values and cool colors represent low *b*-values. Areas of hydrothermal activity are plotted in purple. Light blue lines represent the outline of lakes. Arrows show interpreted magma migration paths from Wicks et al., 2006. Red and blue polygons show the location of the expanding sill and the deflating sill respectively from Chang et al. (2007). MSF = Mt. Sheridan fault, HLF = Hebgen Lake fault, GF = Gallatin fault, and TF = Teton fault.

stress drop of 12 MPa observed for the Hebgen Lake mainshock (Doser, 1985)) in the areas immediately north and south of the fault where we see higher *b*-values.

Another explanation for higher *b*-values within the Yellowstone caldera and in the Norris–Mammoth Corridor (Fig. 2) could be because of the high concentration of hydrothermal features in the area. Hydrothermal waters of Yellowstone circulate through the crust in an intricate system of cracks and are heated from below by a body of crystallizing magma (Fournier, 1989). The presence of extensive hydrothermal activity shows that the crust is very heterogeneous due to the numerous fractures that facilitate the flow of hydrothermal waters through the crust. There is a correlation between higher *b*-values and the location of hydrothermal features in the western half of Yellowstone (Fig. 11). This would indicate that the high *b*-values may be due to both the highly fractured (heterogeneous) crust and the high temperatures as well as high pore pressures that allow hydrothermal fluid flow. Therefore, the high *b*-values could be an

indication of the highly fractured crust that facilitates the movement of hot, hydrothermal fluids. Wall (2005) showed that northeast–southwest and northwest–southeast trending fractures in the 0.64-Ma Lava Creek Tuff provide major flow pathways for hydrothermal fluids at Norris Geyser Basin.

The area of low *b*-values in the southern part of the park where *b*-values are as low as 0.6 ± 0.1 (Fig. 11) can be attributed to high stress accumulation from large Basin-Range faults south of the Yellowstone caldera and outside the dominant influence of the magma system. Stress accumulation would take place mainly on the Mt. Sheridan fault and the Teton fault. The northern segment of the Teton fault appears to extend northward under the 70,000-yr-old Pitchstone Plateau Rhyolite, and the eastern segment of the fault merges into the remains of the ring-fracture system from the 2.05 Ma caldera in Yellowstone National Park (Christiansen and Blank, 1972; Christiansen, 2001). North–south bands of seismicity extend from the northern extent of the Teton fault into the Yellowstone caldera (Fig. 1)

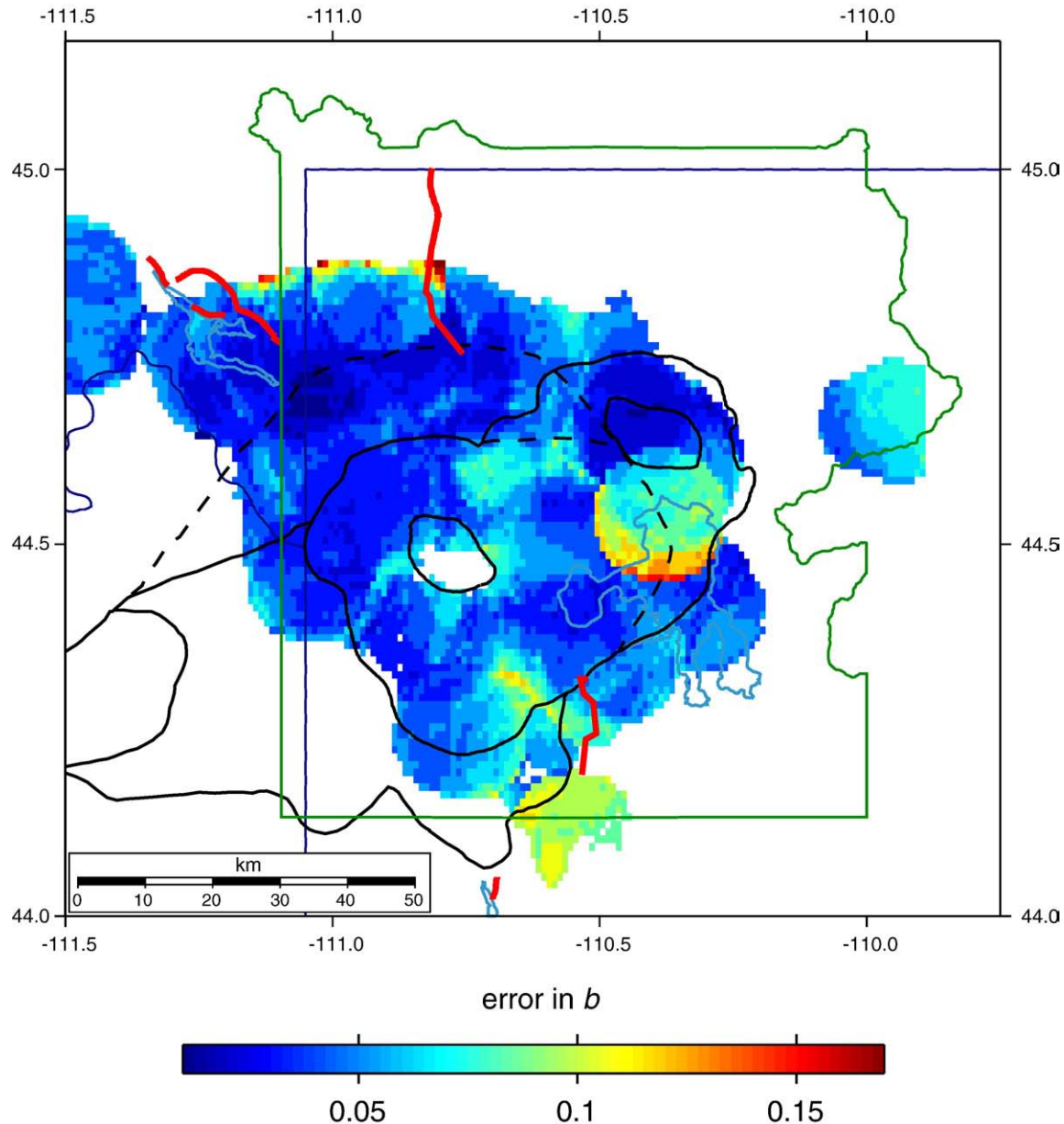


Fig. 12. Errors in the b -value calculations. Calderas I, II, and III are outlined in black. Major Quaternary faults are shown as thick red lines. Symbols are as shown above.

suggesting that these earthquakes occur on existing zones of weakness that may be a buried remnant of the Teton fault.

White et al. (2009-this volume) suggested that the transition from northeast-southwest extension in the northern Teton region to east-west extension in the central and southern Teton region indicates that the stress field along the northern Teton fault may be affected by the stress field of the Yellowstone volcanic system. Given the rapid change in stress orientation around the northern Teton fault segment, the fault may be locked due to westward compression, which would also be loading the fault segment at the same time (White et al., 2009-this volume). Similar results were argued by Hampel and Hetzel (2008) who used finite element modeling to investigate the high rates of Yellowstone caldera uplift and subsidence and its effects on the area south of the Yellowstone caldera and the Teton fault. They show that caldera uplift can induce variations of the stresses of the Teton fault including horizontal compression. Puskas et al. (2007) also recorded reverse motion on the Teton fault using GPS.

It is plausible that the Mt. Sheridan fault could be experiencing higher loading rates as well. The Mt. Sheridan fault is a large north-south striking normal fault bounding the east side of Mt. Sheridan (Fig. 1) and is about 41 km long (Wong et al., 2000). It is believed that prior to the cataclysmic caldera-forming eruptions at Yellowstone, the Mt. Sheridan fault was continuous across the Yellowstone Plateau with the faults to the north of the Yellowstone caldera (Smith and Siegel, 2000).

Scholz (1968), Wyss (1973), Urbancic et al. (1992), Schorlemmer et al. (2004), Schorlemmer and Wiemer (2005), and Schorlemmer et al. (2005) showed that an increase in applied shear stress or an increase in effective stress decreases the b -value. It is proposed here that the low b -values in the southern portion of Yellowstone National Park are due to stress buildup from the East Mt. Sheridan fault and the Teton fault (e.g. Hampel and Hetzel, 2008; White et al., 2009-this volume). The high stress in the area could be due to crustal deformation from the volcanic system in Yellowstone loading the faults. It is not well known how the

large normal faults to the north and south interact with the Yellowstone caldera system, more specifically, whether or not the volcanic system is loading the faults or whether it is absorbing stress.

7. Conclusions

Significant spatial variations in the frequency–magnitude distribution are well-defined in the Yellowstone region and are related to variations in tectonic and volcanic processes. Thirty-nine percent of Yellowstone earthquakes occur in swarms. This corresponds to about 38% of the total seismic moment which equates to an equivalent magnitude of 4.9. Sixty-nine distinct swarms (Fig. 4, Table S1) were identified during the study period, 1984–2006, comprising 8924 earthquakes. Fifty-four of the 69 swarms occur in the east–west band of seismicity that extends from the Hebgen Lake fault to the Norris Geyser Basin (Fig. 4). Swarms vary in duration from 1 to 46 days and have a range of 30 to 722 total events.

The area of high *b*-values just to the north of the Mallard Lake dome, where *b*-values up to 1.5 ± 0.05 are present, is attributed to the presence of a high thermal gradient due to the emplacement of magmatic fluids. Using InSAR data, Wicks et al. (2006) interpreted this area of uplift as due to the emplacement of basaltic magma at ~ 15 km below the surface. Magma intrusion as well as crustal deformation are processes that would alter the frequency–magnitude distribution of earthquakes towards high *b*-values. As magmatic fluids are injected into the system, temperatures are expected to rise around the intrusion and the crust would weaken due to its inability to accumulate high amounts of stress. The high temperature, weakened crust and the expanding sill could cause the formation of numerous small fractures as magma escaped the Yellowstone caldera system. A relatively large number of smaller earthquakes are expected to accompany the formation of small fractures and would alter the frequency–magnitude distribution of earthquakes towards higher *b*-values. This supports the hypothesis that the higher *b*-values in this region are due to the presence of magmatic fluids.

Chang et al. (2007) suggest that the 2004–2006 episode of accelerated uplift of up to 7 cm/yr, occurred in response to a caldera-wide magma recharge of the Yellowstone volcanic system. The unprecedented crustal uplift as well as the increase in thermal gradient due to magma recharge would tend to alter the frequency–magnitude distribution of earthquakes towards a higher *b*-value by not allowing sufficient stress build up on the fractures.

The area of low *b*-values up to 14 km south of the 0.64-Ma caldera rim where *b*-values are as low as 0.6 ± 0.1 is interpreted to be due to high stress in the crust from the loading of both the Mt. Sheridan fault and the Teton fault. This could also be an indication of a relatively strong crust and a thicker seismogenic layer that is resistant to fracture. It is not clear if the high stress in the crust is due to the lack of large earthquakes on the Mt. Sheridan and Teton faults in the recent past or if those faults are being loaded by the crustal deformation from the Yellowstone volcanic system.

With additional data and better broadband seismograph coverage, not only will more information be obtained for Yellowstone earthquakes, but the data will continue to be of higher quality as the network continues to be upgraded to broader frequency recording and location techniques improve. This will allow better determinations of the *b*-value distribution both laterally and with depth as well as over time. This data can be used to better understand what processes are occurring in the crust at Yellowstone and their implications for local earthquake and volcanic hazards.

Acknowledgements

We would like to thank Christine Puskas, Wu-Lung Chang, Michael Jordan, Bonnie Pickering-White, Aaron DeNosaquo, and Katrina DeNosaquo for in-depth discussions. Greg Waite provided the swarm identification algorithm used in this study. We also thank

Jochan Woessner and Danijel Schorlemmer for providing help with the *b*-value analysis program, ZMAP. We would also like to thank Mike Stickney and an anonymous reviewer for their comments and suggestions.

Funding for the project was provided by the National Science Foundation Continental Dynamics Program grants #EAR 9725431, 0314298, and 9316289 and the NSF GEosciences Network (GEON) project, EAR-0724265. Data support was partially provided by the Yellowstone Volcano Observatory. The University of Utah provided computational and technical assistance as well.

Appendix A. Supplementary data

Supplementary data associated with this article can be found, in the online version, at doi:10.1016/j.jvolgeores.2009.08.008

References

- Akaike, H., 1974. A new look at the statistical model identification. *IEEE Trans. Automat. Contr.* 19, 716–723.
- Aki, K., 1965. Maximum likelihood estimate of *b* in the formula $\log N = a - bM$ and its confidence limits. *Bull. Earthq. Res. Inst. Univ. Tokyo* 43, 237–239.
- Bender, B., 1983. Maximum likelihood estimation of *b* values for magnitude grouped data. *Bull. Seismol. Soc. Am.* 73, 831–851.
- Benz, H.M., Smith, R.B., 1984. Simultaneous inversion for lateral velocity variations and hypocenters in the Yellowstone region using earthquake and refraction data. *J. Geophys. Res.* 89, 1208–1220.
- Blackwell, D.D., 1969. Heat-flow determinations in the northwestern United States. *J. Geophys. Res.* 74, 992–1007.
- Chang, W.-L., Smith, R.B., 2002. Integrated seismic-hazard analysis of the Wasatch Front, Utah. *Bull. Seismol. Soc. Am.* 92, 1904–1922.
- Chang, W.-L., Smith, R.B., Wicks, C., Puskas, C.M., Farrell, J., 2007. Accelerated uplift and source models of the Yellowstone caldera, 2004–2006, from GPS and InSAR observations. *Science* 318 (5852), 952–956. doi:10.1126/science.1146842.
- Christiansen, R.L., 1984. Yellowstone magmatic evolution: its bearing on understanding large-volume explosive volcanism. *Explosive Volcanism: Inception, Evolution and Hazards*. National Academy Press, Washington D.C., pp. 84–95.
- Christiansen, R.L., 2001. The Quaternary and Pliocene Yellowstone plateau volcanic field of Wyoming, Idaho, and Montana. *U.S. Geol. Surv. Profess. Pap.* 729-G, 145.
- Christiansen, R.L., Blank Jr., H.R., 1972. Volcanic stratigraphy of the Quaternary rhyolite plateau in Yellowstone National Park. *U.S. Geol. Surv. Profess. Pap.* 516-E, 6.
- DeNosaquo, K., Smith, R.B., Lowry, A.R., 2009. Density and lithospheric strength models of the Yellowstone–Snake River Plain volcanic system from gravity and heat flow data. *J. Volcanol. Geotherm. Res.* 188, 108–127.
- Doser, D.I., 1985. Source parameters and faulting processes of the 1959 Hebgen Lake, Montana, earthquake sequence. *J. Geophys. Res.* 90, 4537–4555.
- Doser, D.I., Smith, R.B., 1983. Seismicity of the Teton–Southern Yellowstone Region, Wyoming. *Bull. Seismol. Soc. Am.* 73, 1369–1394.
- Dzurisin, D., Savage, J.C., Fournier, R.O., 1990. Recent crustal subsidence at Yellowstone caldera, Wyoming. *Bull. Volcanol.* 52, 247–270.
- Eaton, G.P., Christiansen, R.L., Iyer, H.M., Pitt, A.D., Mabey, D.R., Bland Jr., H.R., Zietz, I., Gettings, M.E., 1975. Magma beneath Yellowstone National Park. *Science* 188, 787–796.
- Farrell, J., Smith, R.B., Taira, T., Puskas, C.M., Burlacu, R., Pechmann, J., Heasler, H., Lowenstern, J., 2009. Source properties and deformation analysis of the 2008–2009 Yellowstone Lake earthquake swarm. *Seismol. Res. Lett.* 80 (2), 339.
- Fournier, R.O., 1989. Geochemistry and dynamics of the Yellowstone National Park hydro-thermal system. *Ann. Rev. Earth Planet. Sci.* 17, 13–53.
- Fournier, R.O., 1999. Hydrothermal processes related to movement of fluid from plastic into brittle rock in the magmatic-epithermal environment. *Econ. Geol.* 94 (8), 1193–1212.
- Frolich, C., Davis, S., 1993. Teleseismic *b*-values: or much ado about 1.0. *J. Geophys. Res.* 98, 631–644.
- Guo, Z., Ogata, Y., 1997. Statistical relations between the parameters of aftershocks in time, space, and magnitude. *J. Geophys. Res.* 102, 2857–2873.
- Gutenberg, B., Richter, C.F., 1944. Frequency of earthquakes in California. *Bull. Seismol. Soc. Am.* 34, 185–188.
- Hampel, A., Hetzel, R., 2008. Slip reversals on active normal faults related to the inflation and deflation of magma chambers: numerical modeling with application to the Yellowstone–Teton region. *Geophys. Res. Lett.* 35, L07301. doi:10.1029/2008GL032226.
- Hill, D.P., 1977. A model for earthquake swarms. *J. Geophys. Res.* 82, 1347–1352.
- Hill, D.P., 1992. Temperatures at the base of the seismogenic crust beneath Long Valley Caldera, California, and the Phlegraean Fields Caldera, Italy. In: Gasparini, P., Scarpa, R., Aki, K. (Eds.), *Volcanic Seismology*. Springer-Verlag, Berlin, pp. 432–461.
- Husen, S., Smith, R.B., 2004. Probabilistic earthquake relocation in three-dimensional velocity models for the Yellowstone National Park region, Wyoming. *Bull. Seismol. Soc. Am.* 94, 880–896.
- Husen, S., Smith, R.B., Waite, G.P., 2004a. Evidence for gas and magmatic sources beneath the Yellowstone volcanic field from seismic tomographic imaging. *J. Volcanol. Geotherm. Res.* 131, 397–410.
- Husen, S., Wiemer, S., Smith, R.B., 2004b. Remotely Triggered Seismicity in the Yellowstone National Park region by the 2002 M_w 7.9 Denali fault earthquake, Alaska. *Bull. Seismol. Soc. Am.* 94 (6B), S317–S331.

- Husen, S., Taylor, R., Smith, R.B., Heasler, H., 2004c. Changes in geyser eruption behavior and remotely triggered seismicity in Yellowstone National Park produced by the 2002 M 7.9 Denali fault earthquake, Alaska. *Geology* 32, 537–540.
- Ishimoto, M., Iida, K., 1939. Observations of earthquakes registered with the microseismograph constructed recently. *Bull. Earthq. Res. Inst. Univ. Tokyo* 17, 443–478.
- Jolly, A.D., McNutt, S.R., 1999. Relationship between b -values and maximum depths of seismicity at Martin and Mageik volcanoes, Katmai National Park, Alaska; July 1995–December 1997. *J. Volcanol. Geotherm. Res.* 93, 173–190.
- Kanamori, H., Anderson, D.L., 1975. Theoretical basis of some empirical relations in seismology. *Bull. Seismol. Soc. Am.* 65, 1073–1095.
- Lynch, D.P., 1999. Three-dimensional finite difference tomography of the Basin and Range–Colorado Plateau–Rocky Mountain transition using earthquake and controlled source data: M.S. thesis, University of Utah, Salt Lake City.
- McNutt, S.R., 2005. Volcanic seismology. *Annu. Rev. Earth Planet. Sci.* 33, 461–491.
- Miller, D.S., Smith, R.B., 1999. P and S velocity structure of the Yellowstone volcanic field from local earthquake and controlled source tomography. *J. Geophys. Res.* 104, 15105–15121.
- Mogi, K., 1962. Magnitude–frequency relation for elastic shocks accompanying fractures of various materials and some related problems in earthquakes. *Bull. Earthq. Res. Inst. Univ. Tokyo* 40, 831–853.
- Mogi, K., 1963. Some discussions on aftershocks, foreshocks and earthquake swarms – the fracture of a semi-infinite body caused by an inner stress origin and its relation to the earthquake phenomena. 3. *Bull. Earthq. Res. Inst. Univ. Tokyo* 41, 615–658.
- Morgan, P., Blackwell, D.D., Spafford, R.E., Smith, R.B., 1977. Heat flow measurements in Yellowstone Lake and the thermal structure of the Yellowstone caldera. *J. Geophys. Res.* 82, 3719–3732.
- Murru, M., Montuori, C., Wyss, M., Privitera, E., 1999. The locations of magma chambers at Mt. Etna, Italy, mapped by b -values. *Geophys. Res. Lett.* 26, 2553–2556.
- Pechmann, J.C., Bernier, S.J., Nava, F.M., Terra, and W.J. Arabasz, 2001. Correction of systematic time-dependent coda magnitude errors in the Utah and Yellowstone National Park region earthquake catalogs, 1981–2001, *EOS Trans. AGU* 82(47), Fall Meet. Suppl., Abstract S11B-0572.
- Pelton, J.R., Smith, R.B., 1982. Contemporary vertical surface displacements in Yellowstone National Park. *J. Geophys. Res.* 87, 2745–2761.
- Pitt, A.M., Weaver, C.S., Spence, W., 1979. The Yellowstone Park earthquake of June 30, 1975. *Bull. Seismol. Soc. Am.* 69, 187–205.
- Power, J.A., Wyss, M., Latchman, J.L., 1998. Spatial variations in the frequency–magnitude distribution of earthquakes at Soufrière Hills volcano, Montserrat, West Indies. *Geophys. Res. Lett.* 25, 3653–3656.
- Puskas, C.M., Smith, R.B., Meertens, C.M., Chang, W.L., 2007. Crustal deformation of the Yellowstone–Snake River Plain volcanic system: campaign and continuous GPS observations, 1987–2004. *J. Geophys. Res.* 112, B03401. doi:10.1029/2006JB004325.
- Reasenberg, P., 1985. Second-order moment of central California seismicity, 1969–1982. *J. Geophys. Res.* 90, 5479–5495.
- Sanchez, J.J., McNutt, S.R., Power, J.A., Wyss, M., 2004. Spatial variations in the frequency–magnitude distribution of earthquakes at Mount Pinatubo volcano. *Bull. Seismol. Soc. Am.* 94, 430–438.
- Scholz, C.H., 1968. The frequency–magnitude relation of microfracturing in rock and its relation to earthquakes. *Bull. Seismol. Soc. Am.* 58, 399–415.
- Schorlemmer, D., Wiemer, S., Wyss, M., 2004. Earthquake statistics at Parkfield: 1. Stationarity of b values. *J. Geophys. Res.* 109, B12307. doi:10.1029/2004JB003234.
- Schorlemmer, D., Wiemer, S., 2005. Microseismicity data forecast rupture area. *Nature* 434, 1086.
- Schorlemmer, D., Wiemer, S., Wyss, M., 2005. Variations in earthquake-size distribution across different stress regimes. *Nature* 437, 539–542.
- Shi, Y., Bolt, B.A., 1982. The standard error of the magnitude–frequency b -value. *Bull. Seismol. Soc. Am.* 72, 1677–1687.
- Sibson, R.H., 1982. Fault zone models, heat flow, and the depth distribution of earthquakes in the continental crust of the United States. *Bull. Seismol. Soc. Am.* 72 (1), 151–163.
- Smith, R.B., Arabasz, W.J., 1991. Seismicity of the intermountain seismic belt. In: Slemmons, D.B., Engdahl, E.R., Zoback, M.D., Blackwell, D.D. (Eds.), Neo-tectonics of North America. Geological Society of America, Boulder, Colorado, pp. 185–228.
- Smith, R.B., Braile, L.W., 1994. The Yellowstone hotspot. *J. Volcanol. Geotherm. Res.* 61, 121–187.
- Smith, R.B., Bruhn, R.L., 1984. Intraplate extensional tectonics of the eastern basin-range: inferences on structural style from seismic reflection data, regional tectonics, and thermal-mechanical models of brittle–ductile deformation. *J. Geophys. Res.* 89, 5733–5762.
- Smith, R.B., Sbar, M., 1974. Contemporary tectonics and seismicity of the Western United States with emphasis on the Intermountain Seismic Belt. *Bull. Geol. Soc. Am.* 85, 1205–1218.
- Smith, R.B., Siegel, L., 2000. Windows into the Earth: The Geology of Yellowstone and Grand Teton Parks. Oxford University Press, London. 247.
- Smith, R.B., Shuey, R.T., Pelton, J.R., Bailey, J.P., 1977. Yellowstone Hot Spot, crustal properties from new earthquake and magnetic data. *J. Geophys. Res.* 82, 3665–3676.
- Smith, R.B., Jordan, M., Steinberger, R., Puskas, C.M., Farrell, J., Waite, G.P., Husen, S., Chang, W., O'Connell, R., Klingele, E., 2009. Geodynamics of the Yellowstone hotspot and mantle plume: seismic and GPS imaging, kinematics, and mantle flow. *J. Volcanol. Geotherm. Res.* 188, 26–56.
- Sykes, L.R., 1970. Earthquake swarms and sea-floor spreading. *J. Geophys. Res.* 75, 6598–6611.
- Taira, T., Smith, R.B., Chang, W.-L., 2009. Seismic evidence for dilatational source deformations accompanying the 2004–2008 Yellowstone accelerated uplift episode. *J. Geophys. Res.* (in press).
- Toda, Shinji, Stein, R.S., Sagiya, T., 2002. Evidence from the AD 2000 Izu islands earthquake swarm that stressing rate governs seismicity. *Nature* 419, 58–61.
- Urbancic, T.I., Trifunovic, C.I., Long, J.M., Toung, R.P., 1992. Space-time correlations of b values with stress release. *Pure Appl. Geophys.* 139, 449–462.
- Utsu, T., 1965. A method for determining the value of b in a formula $\log N = a - bM$ showing the magnitude frequency for earthquakes. *Geophys. Bull. Hokkaido Univ.* 13, 99–103.
- Utsu, T., 1992. On seismicity. Report of the Joint Research Institute for Statistical Mathematics: Inst. For Stat. Math., Tokyo, vol. 34, pp. 139–157.
- Utsu, T., 1999. Representation and analysis of the earthquake size distribution: a historical review and some approaches. *Pure Appl. Geophys.* 155, 509–535.
- Vidale, J.E., Boyle, K.L., Shearer, P.M., 2006. Crustal earthquake bursts in California and Japan: their patterns and relation to volcanoes. *Geophys. Res. Lett.* 33, L20313. doi:10.1029/2006GL027723.
- Waite, G.P., 1999. Seismicity of the Yellowstone Plateau: space–time patterns and stresses from focal mechanism inversion: M.S. thesis, University of Utah, Salt Lake City.
- Waite, G.P., Smith, R.B., 2002. Seismic evidence for fluid migration accompanying subsidence of the Yellowstone caldera. *J. Geophys. Res.* 107 (B9), 2177. doi:10.1029/2001JB000586.
- Wall, B.R., 2005. Surface and subsurface hydrothermal flow pathways at Norris Geyser Basin, Yellowstone National Park, *Eos Trans. AGU*, 86(52), Fall Meet. Suppl. Abstract T23B-0544.
- Warren, N.W., Latham, G.V., 1970. An experimental study of thermally induced microfracturing and its relation to volcanic seismicity. *J. Geophys. Res.* 75, 4455–4464.
- White, B.J.P., Smith, R.B., Husen, S., Farrell, J., Wong, I., 2009. Seismicity and earthquake hazard analysis of the Teton–Yellowstone region, Wyoming. *J. Volcanol. Geotherm. Res.* 188, 277–296.
- Wicks, C., Thatcher, W., Dzurisin, D., Svarc, J., 2006. Uplift, thermal unrest and magma intrusion at Yellowstone caldera. *Nature* 440, 72–75.
- Wiemer, S., 2001. A software package to analyze seismicity: ZMAP. *Seismol. Res. Lett.* 72, 373–382.
- Wiemer, S., Benoit, J.P., 1996. Mapping the b -value anomaly at 100 km depth in Alaska and New Zealand subduction zones. *Geophys. Res. Lett.* 24, 189–192.
- Wiemer, S., McNutt, S.R., 1997. Variations in the frequency–magnitude distribution with depth in two volcanic areas: Mount St. Helens, Washington, and Mt. Spurr, Alaska. *Geophys. Res. Lett.* 24, 189–192.
- Wiemer, S., Wyss, M., 1997. Mapping the frequency–magnitude distribution in asperities: an improved technique to calculate recurrence times? *J. Geophys. Res.* 102, 15115–15128.
- Wiemer, S., Wyss, M., 2000. Minimum magnitude of completeness in earthquake catalogs: examples from Alaska, the western United States, and Japan. *Bull. Seismol. Soc. Am.* 90 (4), 859–869.
- Wiemer, S., Wyss, M., 2002. Mapping spatial variability of the frequency–magnitude distribution of earthquakes. *Adv. Geophys.* 45, 259–302.
- Wiemer, S., McNutt, S.R., Wyss, M., 1998. Temporal and three-dimensional spatial analyses of the frequency–magnitude distribution near Long Valley Caldera, California. *Geophys. J. Int.* 134, 409–421.
- Woessner, J., Wiemer, S., 2005. Assessing the quality of earthquake catalogues: estimating the magnitude of completeness and its uncertainty. *Bull. Seismol. Soc. Am.* 95 (2), 684–698. doi:10.1785/0120040007.
- Wong, I., S. Olig, and M. Dober, 2000, Preliminary Probabilistic Seismic Hazard Analysis; Island Park, Grassy Lake, Jackson Lake, Palisades, and Ririe Dams, U.R.S. Griener Woodward Clyde, Final report prepared for the Bureau of Reclamation, 40 pages.
- Wyss, M., 1973. Towards a physical understanding of the earthquake frequency distribution. *Geophys. J. R. Astron. Soc.* 31, 341–359.
- Wyss, M., Shimazaki, S., Wiemer, S., 1997. Mapping active magma chambers beneath the off-*to* volcano, Japan. *J. Geophys. Res.* 102, 413–420.
- Wyss, M., Klein, F., Nagamine, K., Wiemer, S., 2001. Anomalously high b -values in the South Flank of Kilauea volcano, Hawaii: evidence for the distribution of magma below Kilauea's East rift zone. *J. Volcanol. Geotherm. Res.* 106, 23–37.
- Youngs, R.R., Swan, F.H., Power, M.S., Schwartz, D.P., Green, R.K., 1987. Probabilistic analysis of earthquake ground shaking hazard along the Wasatch Front, Utah. In: Gori, P.L., Hays, W.W. (Eds.), Assessment of Regional Earthquake Hazards and Risk along the Wasatch Front, Utah. USGS, Reston, VA, pp. M1–M110.

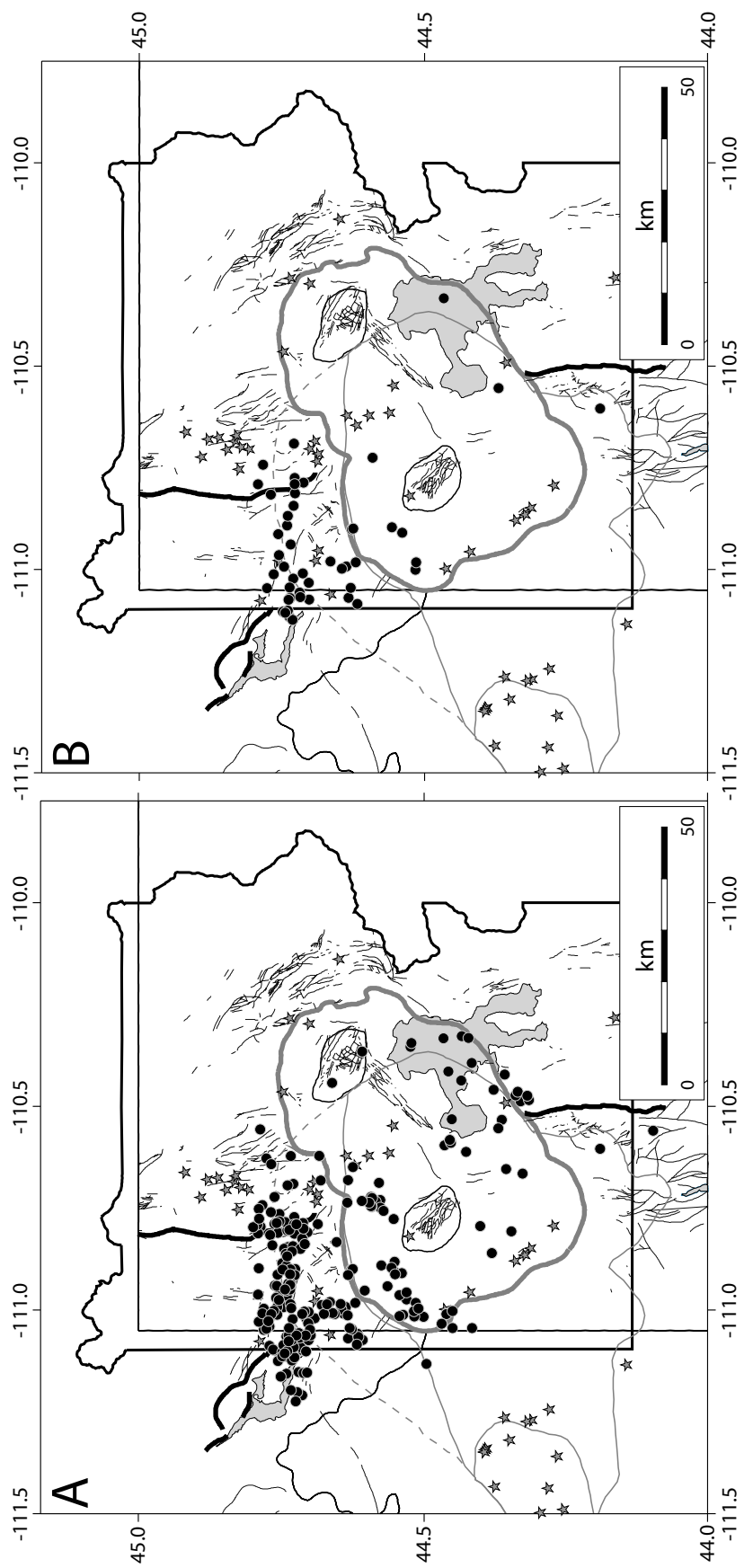


Figure S1. Yellowstone swarm locations identified while using the a) 10-minute minimum definition of a swarm and b) 50-minute minimum definition of a swarm. Mean locations for the swarms are shown by black circles. Post-caldera volcanic vents are shown as gray stars. The 0.64-Ma caldera is outlined as a thick gray line and the 1.3-Ma and 2.05-Ma caldera boundaries are outlined as thin gray lines, with the possible northern extent of the 2.05-Ma caldera shown with a dashed gray line. Quaternary faults after Christiansen (2001) are shown as thin black lines. Major Quaternary faults are shown as thick black lines.

Table S1 - Table of Yellowstone earthquake swarms

#	Start Day	End Day	Dur	Lon	Lat	EQ/Day _{max}	Mag _{max}	No. EQ
1	3/1/1985	3/11/1985	11	-110.7495	44.7884	71	2.77	148
2	10/3/1985	11/17/1985	46	-110.9995	44.6422	85	3.72	462
3	11/24/1985	12/10/1985	17	-111.0050	44.6503	11	3.08	52
4	9/29/1989	10/3/1989	5	-111.0635	44.7243	37	2.16	67
5	10/24/1989	11/1/1989	8	-111.0770	44.7411	50	2.28	68
6	2/26/1990	3/9/1990	12	-111.0765	44.6385	84	2.11	233
7	5/2/1994	5/4/1994	3	-111.0815	44.7436	38	2.26	54
8	9/9/1994	9/17/1994	9	-111.0295	44.7356	33	2.11	52
9	6/25/1995	7/9/1995	15	-110.9080	44.6329	170	2.84	439
10	7/11/1995	7/21/1995	11	-110.9060	44.6303	41	2.35	90
11	11/27/1995	12/8/1995	12	-110.8985	44.7461	43	3.05	192
12	10/11/1996	11/8/1996	29	-110.7820	44.7331	68	2.83	281
13	4/27/1997	5/12/1997	16	-110.7910	44.7455	17	2.18	44
14	6/6/1997	6/27/1997	22	-110.8195	44.7324	140	3.76	363
15	7/7/1997	7/21/1997	15	-110.7935	44.7175	27	2.61	52
16	8/12/1997	8/13/1997	2	-111.0810	44.7075	76	1.90	91
17	12/25/1997	12/30/1997	6	-111.0395	44.7082	45	2.59	64
18	5/26/1998	5/28/1998	3	-110.7955	44.7673	34	2.21	35
19	9/27/1998	9/30/1998	4	-111.0550	44.7050	44	2.27	49
20	9/27/1998	10/4/1998	8	-110.3400	44.4711	52	3.80	159
21	11/10/1998	12/1/1998	22	-111.0915	44.6229	50	2.55	189
22	1/1/1999	1/13/1999	13	-110.8225	44.7747	16	2.69	61
23	5/11/1999	5/19/1999	9	-111.0720	44.7461	15	2.34	31
24	5/17/1999	5/31/1999	15	-110.9870	44.6702	19	2.40	70
25	6/13/1999	7/16/1999	34	-111.0000	44.7517	112	4.19	722
26	6/13/1999	6/25/1999	13	-111.1105	44.7536	42	2.31	143
27	6/27/1999	7/7/1999	11	-111.1195	44.7486	9	2.07	38
28	7/31/1999	8/28/1999	29	-110.9715	44.7604	119	3.14	586
29	8/7/1999	8/14/1999	8	-111.1225	44.7424	136	2.17	162
30	8/27/1999	8/27/1999	1	-110.6025	44.4692	35	4.82	35
31	10/3/1999	10/21/1999	19	-110.9200	44.7617	37	3.03	101
32	10/28/1999	10/28/1999	1	-111.0165	44.6808	48	1.55	48
33	12/21/1999	12/26/1999	6	-110.9465	44.7666	19	2.76	38
34	1/25/2000	1/30/2000	6	-111.0745	44.7231	49	2.27	59
35	3/21/2000	4/13/2000	24	-111.0185	44.7698	40	2.16	278
36	7/25/2000	8/18/2000	25	-110.7975	44.7971	54	2.72	211
37	10/24/2000	10/27/2000	4	-111.1305	44.7368	29	2.18	51
38	11/23/2000	11/26/2000	4	-110.6975	44.7343	82	3.76	93
39	12/24/2000	12/28/2000	5	-110.8500	44.7349	34	2.51	54
40	1/16/2001	1/25/2001	10	-111.0520	44.6347	130	2.40	320
41	2/26/2001	3/2/2001	5	-111.0165	44.7188	29	1.94	54
42	4/30/2001	5/4/2001	5	-110.9420	44.7386	17	1.91	37
43	6/19/2001	6/28/2001	10	-110.9075	44.7529	10	2.48	35
44	9/6/2001	9/10/2001	5	-111.0180	44.7623	16	0.99	34
45	11/20/2001	11/22/2001	3	-110.8690	44.7473	18	1.29	31
46	11/30/2001	1/9/2002	41	-111.0530	44.7815	49	3.13	480

Table S1 - Table of Yellowstone earthquake swarms continued

#	Start Day	End Day	Dur	Lon	Lat	EQ/Day_{max}	Mag_{max}	No. EQ
47	1/15/2002	1/17/2002	3	-110.7320	44.5961	56	2.78	60
48	1/29/2002	2/2/2002	5	-111.0090	44.7685	22	0.82	49
49	8/9/2002	8/15/2002	7	-110.9925	44.7392	10	1.46	30
50	10/8/2002	10/12/2002	5	-110.5610	44.3746	64	3.14	110
51	11/3/2002	11/7/2002	5	-110.9590	44.6092	18	2.47	45
52	11/3/2002	11/10/2002	8	-110.7970	44.7330	31	1.54	59
53	11/3/2002	11/10/2002	8	-111.1080	44.7449	48	2.89	67
54	12/5/2002	12/10/2002	6	-110.8750	44.7449	283	3.32	331
55	1/3/2003	1/13/2003	11	-111.0075	44.5208	43	2.48	85
56	1/29/2003	2/13/2003	16	-110.9895	44.5196	31	2.92	79
57	2/5/2003	2/7/2003	3	-111.0020	44.7380	22	1.17	35
58	4/12/2004	4/20/2004	9	-110.9519	44.7449	295	2.60	429
59	7/16/2004	7/18/2004	3	-111.1771	44.7611	20	2.22	35
60	6/1/2005	6/8/2005	8	-111.1199	44.7542	16	2.08	51
61	8/14/2005	8/24/2005	11	-110.9968	44.6304	13	1.76	53
62	2/22/2006	2/22/2006	1	-110.9700	44.5408	42	1.95	42
63	4/5/2006	4/6/2006	2	-110.6176	44.1998	37	2.43	74
64	5/18/2006	5/26/2006	9	-110.9892	44.7642	14	2.50	45
65	6/11/2006	6/21/2006	11	-111.0576	44.7468	28	2.12	81
66	6/12/2006	6/15/2006	4	-110.9100	44.5669	37	2.26	55
67	7/10/2006	7/11/2006	2	-110.7897	44.5632	25	2.83	31
68	10/14/2006	10/15/2006	2	-110.9231	44.5489	54	2.61	74
69	11/4/2006	11/7/2006	4	-111.0474	44.4792	36	2.57	47